NAVAL POSTGRADUATE SCHOOL

MONTEREY, CALIFORNIA

THESIS

RADAR TARGET RECOGNITION USING BISPECTRUM CORRELATION

by

Zachary K. Cole

June 2007

Thesis Advisor: Brett Borden
Second Reader: Donald Walters

Approved for public release; distribution is unlimited

THIS PAGE INTENTIONALLY LEFT BLANK

REPORT DOCUMENTATION PAGE		Form Approved OMB No. 0704-0188

1. AGENCY USE ONLY *(Leave blank)*	2. REPORT DATE	3. REPORT TYPE AND DATES COVERED
	June 2007	Master's Thesis

4. TITLE AND SUBTITLE Radar Target Recognition Using Bispectrum Correlation	5. FUNDING NUMBERS
6. AUTHOR(S) Cole, Zachary K.	
7. PERFORMING ORGANIZATION NAME(S) AND ADDRESS(ES) Naval Postgraduate School Monterey, CA 93943-5000	8. PERFORMING ORGANIZATION REPORT NUMBER
9. SPONSORING /MONITORING AGENCY NAME(S) AND ADDRESS(ES) N/A	10. SPONSORING/MONITORING AGENCY REPORT NUMBER

11. SUPPLEMENTARY NOTES The views expressed in this thesis are those of the author and do not reflect the official policy or position of the Department of Defense or the U.S. Government.

12a. DISTRIBUTION / AVAILABILITY STATEMENT	12b. DISTRIBUTION CODE
Approved for public release; distribution is unlimited.	A

13. ABSTRACT (maximum 200 words)

Ship commanders and pilots make life or death decisions based on the information they have at their disposal at the instant a decision is made. One component of that information is whether a radar contact is an enemy or a friend. Various systems exist which try to answer that question based on the characteristics of signals emitted or scattered from the contact. The goal is to maximize the accuracy of identification in order to build trust that when the system tells the operator the contact is an incoming friendly, he knows that it is.

This thesis examines the technique of using the bispectrum of backscattered radar energy to identify a contact. Bispectra allow the examination of multiple scattering contributions to the return. This technique is compared to one using radar range profiles. A library of sample radar signatures is built using computational radar cross section estimation tools and 3-D model aircraft. This library is the basis of a series of simulations with aircraft at multiple aspects and configurations to determine whether using the bispectrum enhances the performance of identification systems using range profiles. It is determined that a bispectrum method meets or exceeds the identification accuracy of a range profile method especially with high-bandwidth systems.

14. SUBJECT TERMS	15. NUMBER OF PAGES
Bispectrum, Non-Cooperative Target Recognition (NCTR) Techniques, Range Profile	97
	16. PRICE CODE

17. SECURITY CLASSIFICATION OF REPORT	18. SECURITY CLASSIFICATION OF THIS PAGE	19. SECURITY CLASSIFICATION OF ABSTRACT	20. LIMITATION OF ABSTRACT
Unclassified	Unclassified	Unclassified	UL

NSN 7540-01-280-5500 Standard Form 298 (Rev. 2-89)
Prescribed by ANSI Std. 239-18

THIS PAGE INTENTIONALLY LEFT BLANK

Approved for public release; distribution is unlimited

RADAR TARGET RECOGNITION USING BISPECTRUM CORRELATION

Zachary K. Cole
Lieutenant, United States Navy
B.S., United States Naval Academy, 2002

Submitted in partial fulfillment of the
requirements for the degree of

MASTER OF SCIENCE IN PHYSICS

from the

NAVAL POSTGRADUATE SCHOOL
June 2007

Author: Zachary K. Cole

Approved by: Brett Borden
Thesis Advisor

Donald Walters
Second Reader

James Luscombe
Chairman, Department of Physics

THIS PAGE INTENTIONALLY LEFT BLANK

ABSTRACT

Ship commanders and pilots make life or death decisions based on the set of information they have at their disposal at the instant a decision is made. One component of that information is the question of whether a radar contact is an enemy or a friend. Various systems exist which try to answer that question based on the characteristics of signals emitted or scattered from the contact. Any hesitation made by the operator as a result of not trusting the identification being presented by his system can be fatal. The goal is to maximize the quality of the information he receives in order to build the trust that when the system tells the operator the contact is an incoming friendly, he knows that it is.

This thesis examines the technique of using the bispectrum of backscattered radar energy to identify a contact. Bispectra allow the examination of multiple scattering contributions to the backscattered energy. This technique is compared to one using radar range profiles. A library of sample radar signatures is built using computational radar cross section estimation tools and 3-D model aircraft. This library is the basis of a series of simulations with aircraft at multiple aspects and configurations to determine whether using the bispectrum enhances the performance of identification systems using range profiles. It is determined that a bispectrum method meets or exceeds the identification accuracy of the range profile method especially with high-bandwidth systems.

THIS PAGE INTENTIONALLY LEFT BLANK

TABLE OF CONTENTS

I. INTRODUCTION....1
A. MOTIVATION....1
1. Detect-to-Engage Sequence....1
2. The Price of Failure....2
B. ORGANIZATION....3
1. Chapter Descriptions....3
2. Thesis Objective....3

II. OVERVIEW OF RADAR PRINCIPLES....5
A. BASIC HARDWARE SETUP....5
B. ANTENNA DESIGN....6
C. THE RADAR EQUATION....7
D. RESOLUTION....8
1. Bearing Resolution....8
2. Range Resolution....9

III. ELECTROMAGNETIC SCATTERING....11
A. ELECTROMAGNETIC WAVES....11
B. SCATTERING....13
1. Physical Optics....14
2. Physical Theory of Diffraction....16
3. Shooting and Bouncing Rays....17

IV. CONTACT IDENTIFICATION....19
A. IDENTIFICATION FRIEND OR FOE....19
B. NON-COOPERATIVE TARGET RECOGNITION....21
1. Modulation Schemes....21
2. Inverse Synthetic Aperture Radar....22
3. Range Profiles....23
4. Bispectrum Profiles....25
C. 3 POINT SCATTERERS EXAMPLE....26

V. SIMULATION....29
A. BUILDING THE LIBRARY....29
1. Scenario....29
2. Aircraft....30
3. Aspect Angles....31
4. Radars....32
5. RCS Tools....32
6. Processing of Frequency Domain Data....33
B. RUNNING THE SIMULATION....33
1. Test Cases....33
2. Range Profile Correlation....34
3. Bispectrum Correlation....35

4. Program Flow 35
VI. ANALYSIS 37
A. SIDE BY SIDE COMPARISON 37
B. THE EFFECT OF BANDWIDTH 38
C. ROTATIONAL VARIANCE 40
D. CONFIGURATION CHANGES 43
E. SIMULATION RESULTS 44
1. High Bandwidth Results 44
2. Low Bandwidth Results 49
VII. CONCLUSIONS 55
A. SUMMARY 55
B. EFFECTIVENESS 55
C. ADDITIONAL CONSIDERATIONS 56
APPENDIX 59
A. AIRCRAFT USED IN SIMULATION 59
B. LIST OF TEST CASES 62
C. BISPECTRUM CODE 63
D. SIMULATION CODE 63
E. INDIVIDUAL SIMULATION RESULTS 73
LIST OF REFERENCES 79
INITIAL DISTRIBUTION LIST 81

LIST OF FIGURES

Figure 1. Simple Pulsed Radar [6] 6
Figure 2. Sample beam pattern for rectangular aperature. [6] 7
Figure 3. Range resolution using simplified waveform 9
Figure 4. FM chirp representation. [6] 9
Figure 5. Representation of an Electromagnetic Wave. [11] 12
Figure 6. Scattering of a Plane Wave on a PEC Sphere [14]. 14
Figure 7. Facetization of a Surface [18] 15
Figure 8. Scattering from a Diffracting Edge [19] 16
Figure 9. Rays Interacting With F-15 Model [18] 18
Figure 10. Example of IFF Antenna Attached to the SPS-49 Radar [21] 20
Figure 11. Sample ISAR Image of a Boeing 727 airliner [5] 23
Figure 12. Simulated Range Profile of an F/A-18 25
Figure 13. Illustration of 3 Point Scatterers Example [11] 26
Figure 14. Range Profile of 3 Point Scatterers [11] 27
Figure 15. Characteristic Bispectrum Plot of 3 point Scatterers [11] 28
Figure 16. Simulation Scenario 29
Figure 17. Model and Wireframe of F/A-18E Super Hornet 30
Figure 18. Range of Angles Considered 31
Figure 19. Range Profile and Bispectrum Plot of A320 37
Figure 20. Range Profiles of F-15E at HBW and LBW 38
Figure 21. Bispectrum Plots of F-15E at HBW and LBW 39
Figure 22. Rotational Variance of F/A-18E Range Profiles 40
Figure 23. Rotational Variance of F/A-18E Bispectrum Plots 41
Figure 24. Multi-Configuration Range Profiles of F-16C 43
Figure 25. Multi-Configuration Bispectrum Plots of F-16C 44
Figure 26. Airbus A320 59
Figure 27. EA-6B Prowler 59
Figure 28. F-4N Phantom II 59
Figure 29. F-14D Tomcat 60
Figure 30. F-15E Strike Eagle 60
Figure 31. F-16C Falcon 60
Figure 32. F/A-18E Super Hornet 60
Figure 33. MiG-29A Fulcrum 61
Figure 34. Su-27 Flanker B 61
Figure 35. UH-60L Black Hawk 61

THIS PAGE INTENTIONALLY LEFT BLANK

LIST OF TABLES

Table 1. Rotational High Bandwidth Profile Correlations....42
Table 2. Rotational Low Bandwidth Profile Correlations....42
Table 3. Rotational High Bandwidth Bispectrum Correlations....42
Table 4. Rotational Low Bandwidth Bispectrum Correlations....42
Table 5. HBW Range Profile Simulation With Stock Aircraft at Far Angles....45
Table 6. HBW Range Profile Simulation With Stock Aircraft at Near Angles....45
Table 7. HBW Bispectrum Simulation With Stock Aircraft at Far Angles....46
Table 8. HBW Bispectrum Simulation With Stock Aircraft at Near Angles....46
Table 9. HBW Range Profile Simulation With Armed Aircraft at Exact Angles....47
Table 10. HBW Range Profile Simulation With Armed Aircraft at Near Angles....48
Table 11. HBW Bispectrum Simulation With Armed Aircraft at Exact Angles....48
Table 12. HBW Bispectrum Simulation With Armed Aircraft at Near Angles....49
Table 13. LBW Range Profile Simulation With Stock Aircraft at Far Angles....50
Table 14. LBW Range Profile Simulation With Stock Aircraft at Near Angles....50
Table 15. LBW Bispectrum Simulation With Stock Aircraft at Far Angles....51
Table 16. LBW Bispectrum Simulation With Stock Aircraft at Near Angles....51
Table 17. LBW Range Profile Simulation With Armed Aircraft at Exact Angles....52
Table 18. LBW Range Profile Simulation With Armed Aircraft at Near Angles....52
Table 19. LBW Bispectrum Simulation With Armed Aircraft at Exact Angles....53
Table 20. LBW Bispectrum Simulation With Armed Aircraft at Near Angles....53
Table 21. Results Summary for High Bandwidth Simulation....56
Table 22. Results Summary for Low Bandwidth Simulation....56

THIS PAGE INTENTIONALLY LEFT BLANK

ACKNOWLEDGMENTS

I'd like to thank my thesis advisor, Dr. Brett Borden, whose guidance and knowledge were essential in this research, and my second reader, Dr. Donald Walters, who provided valuable insight into the problem. I want to thank Jiunn Wah Yeo whose thesis work provided the starting point for my research. Walton C. Gibson of Tripoint Industries and Marv Mays of Mesh Factory helped resolve some technical difficulties during the simulation. Janis Higginbotham aided me in the formatting and editing of the thesis.

I especially want to thank my coworkers in the inverse scattering lab, LT Jerry Kim and LT Armando Lucrecio. Their friendship and conversation helped me stay sane during the many long hours of computer programming. I would like to thank my parents, CAPT (ret) Thomas and Denise Cole of Virginia Beach, VA, whose encouragement was a necessary part of this process. Finally, I'd like to thank my lovely fiancé, LT Lauren Zapf, for the motivation she gives me and the love she shows me every day.

THIS PAGE INTENTIONALLY LEFT BLANK

I. INTRODUCTION

A. MOTIVATION

The importance of having accurate information on the battlefield cannot be underestimated. Critical decisions must be made whether all the pertinent information is available or not. The decision to shoot down an incoming aircraft sometimes must be made without knowing exactly what that aircraft is. Inaccurate or unavailable identification information can therefore lead to instances where friendly or neutral forces are fired upon inadvertently. Improving the quality of information provided by the combat systems will enhance our warfighting capabilities allowing our warfighters to have a more accurate view of the battle space.

1. Detect-to-Engage Sequence

Every naval tactician is taught in their basic naval science class the detect-to-engage sequence. It is the sequence of steps through which every successful encounter with the enemy progresses, whether the sailor is on guard duty with a rifle or a Tactical Action Officer (TAO) on an Aegis Cruiser. I will look at this process from the point of view of the TAO. The first step in the process is detection. There are many ways a modern warship can detect a target, but a common method is via radar. Once the radar detects a target, it will enter it into its database and start to track it. Combining information from all available sensors, identification of the contact can be accomplished. Based on the current rules of engagement, a threat assessment of the contact is performed. A contact deemed hostile will be paired with a particular weapon or platform to commence the engagement. Following the engagement, a damage assessment must be performed to determine if an additional engagement is necessary.

Each of these steps is not always a formalized process and the particular order can be rearranged to a certain extent. Our advancing weapons technology has made the engagement an increasingly successful part of the process, and modern radars provide a well over the horizon look at the airspace. The most troubling part lies with the identification and threat assessment of the contact. There is still an element of

subjectivity with the threat assessment; it can be based on experience and intuition and is very situation dependent. Many different techniques exist to identify contacts, but none are without flaw. Also, an enemy's efforts in deception can change characteristics that would otherwise reveal their identity. These elements of the sequence are big parts of what keeps the process from being fully automated. Improving the reliability of the identification phase will also enhance the assessment of the threat.

2. The Price of Failure

There have been a number of incidents in modern American history which illustrate the consequences of having inaccurate identification information. These cases not only lead to the destruction of millions of dollars in property, but also lead to the deaths of many innocent civilians or friendly military forces.

1988 USS Vincennes incident – On June 2, 1988, the Aegis cruiser USS Vincennes shot down Iran Air Flight 655. The Vincennes and the frigate USS Elmer Montgomery were engaged in a surface gun battle with Iranian gunboats. The Iranian Airbus A300 took off from Bandar Abbas and was misidentified by the Vincennes as an F14 fighter aircraft. Despite flying in a commercial flight path, the aircraft was labeled hostile and was shot down by two standard missiles from the Vincennes. All 290 persons aboard were killed [1].

1994 Iraqi no-fly zone – On April 14, 1994, two Air Force F-15 fighters shot down two American MH-60 Blackhawk helicopters in the no-fly zone in northern Iraq. The helicopters were not identifying themselves properly via their IFF system, (see Chapter IV) and they were misidentified electronically and visually by the fighters and surveillance aircraft. 26 military and civilian personnel lost their lives [2].

2003 Downing of British Tornado – On March 23, 2003, a U.S. Patriot missile battery shot down a British GR4 Tornado aircraft after misidentifying it as an incoming missile. The GR4 was returning from a mission in Iraq. The Patriot missiles can operate in mostly autonomous modes where automatic identifications play a major role in the engagement [3]. Both pilot and navigator were killed.

B. ORGANIZATION

1. Chapter Descriptions

This thesis examines a way to improve the accuracy of radar contact identification. Chapter II begins with an overview of basic radar concepts. Included is a brief discussion of different signal forms and high resolution techniques which enable the later technologies. Chapter III deals with how the radar waves actually interact with the aircraft and scatter back to the receiver. The different contributions to the radar backscatter are examined with a simple example. Chapter IV gives an overview of identification methods of radar contacts. Both cooperative and non-cooperative classification methods are examined including the shortcomings of the current methods. In addition the technique of using the bispectrum of the radar signal to improve the accuracy of classifications is described. A method of how to calculate the bispectrum and an example using simple shapes is shown. Chapter V describes the simulation that was performed to test the hypothesis that the use of the bispectrum will improve classification accuracy. A discussion of the creation of a library of aircraft signatures and a selection of sample test cases is included. Chapter VI provides results from the simulation. Additional observations using the library of signatures are made. Conclusions follow in Chapter VII to summarize the findings and to recommend further examination.

2. Thesis Objective

A library of radar backscattered data from various models of military and civilian aircraft is desired to test various classification methods. This library will be accessible for future work beyond this thesis. A comparison of radar range profile based classification methods versus a method based on the bispectrum of the responses is performed. The goal is to improve the reliability of automated radar based classification techniques by demonstrating a promising method to enhance current methods.

THIS PAGE INTENTIONALLY LEFT BLANK

II. OVERVIEW OF RADAR PRINCIPLES

A basic understanding of how a radar system works is helpful in understanding the goals of this thesis. The word radar began as an acronym for Radio Detection and Ranging but has become so pervasive that it is now a word by itself. Radar is a system which determines a contact's range, bearing, velocity, and other information by emitting electromagnetic energy and measuring the energy that reflects from the contact. Radar signals can be based on pulses which alternate between transmitting and receiving energy, or they can be continuous wave (CW) systems which constantly transmit and receive simultaneously.

The wide scale use of radar began in World War II. A well-known system was the British Chain Home radar which allowed advance notice of attacking German fighters and bombers [4]. British fighters were able to be vectored directly to where the incoming planes were, therefore greatly enhancing their effectiveness. The United States was also working on its own radar at the time. The invention of the magnetron to deliver high power, coherent microwaves, and the duplexer switch enabled construction of a pulsed radar which was much smaller than the original lower frequency radars [5]. Higher frequency radars allow the use of smaller antennas which make the system portable and more easily mounted on mobile platforms. Radar technology has drastically improved over the years with the advancement of signal processing techniques. Also, complicated antenna designs allow energy to be directed to desired locations without mechanically moving the antenna.

A. BASIC HARDWARE SETUP

Because of the spreading of electromagnetic waves, the reflected and received energy after the round trip is multiple orders of magnitude less than the transmitted energy. The receiver therefore must be a very sensitive piece of equipment. A duplexer allows it to be connected to the same antenna of the transmitter without being overwhelmed by the transmitted energy. A basic layout of a pulsed radar is depicted in Figure 1. Waveforms from the pulse generator allow varying levels of resolution and

will be discussed in the next section. Heterodyne mixing is done before transmitting and after receiving to step up an intermediate frequency to a higher frequency. This is done because a higher frequency transmitted may have better transmission and reflection characteristics, but the lower intermediate frequency is easier to manage for the electronic signal processing components. Various displays have been developed over the years beginning with phosphor scopes, and now high-tech multifunction computer displays found on modern warships. Filters and low noise amplifiers ensure the detector receives the right amount of power for detection without saturating or damaging components.

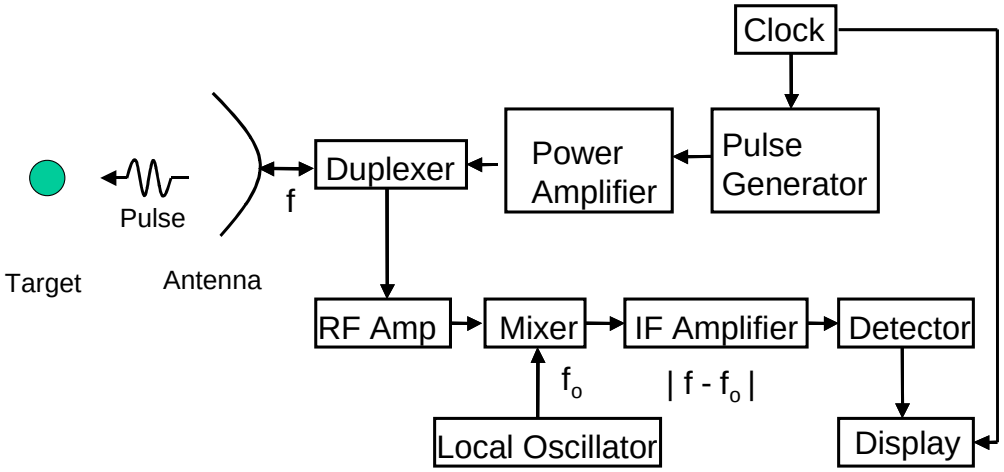

Figure 1. Simple Pulsed Radar [6]

B. ANTENNA DESIGN

After the energy is produced by the system, the antenna is what transfers that energy into the environment. The particular antenna design is motivated by the intended use of the system. These antennas could be simple dipoles to be used as a 360-degree proximity warning device for ships similar to Christian Huelsmeyer's ship avoidance system in 1904 [5]. Or the antenna could be a complex, electronically steered, phased array antenna found on modern warships and aircraft generating a narrow beam. Traditional radar antennas consist of a feed horn at the end of a waveguide which directs energy to a parabolic dish. The shape of the parabolic dish largely determines the beam pattern formed. The electrical current distribution excited on the dish creates the radiation pattern and in general, the far-field beam pattern is the 2-dimensional Fourier

Transform of the aperture shape [7]. Because of the Fourier relationship between spatial frequency and length, wide dimensions provide narrow beams and narrow dimensions provide wider beams. Also, by adding a windowing function to the energy directed at the aperture, the sidelobes of the signal can be reduced, albeit at the cost of a wider main lobe. By grouping multiple elements together in an array, areas of constructive and destructive interference create a beam pattern that can be steered by changing the phase difference of the transmitted waveform between elements. A sample beam pattern showing sidelobes is displayed in Figure 2.

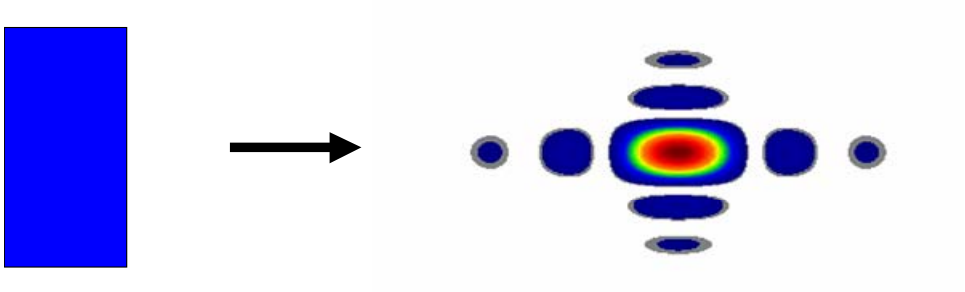

Figure 2. Sample beam pattern for rectangular aperture. [6]

C. THE RADAR EQUATION

The radar equation estimates the theoretical maximum range at which a radar can detect a target. If we take the power density of the transmitted antenna to be P_T then, taking into account the gain of the antenna, G, and spherical spreading of the waves, the power density at the target is given by [5]:

$$P_{\text{target}} = \frac{P_T G}{4\pi R^2} \tag{1}$$

This is the power available to be scattered from the target. The amount of energy scattered from the target is given in terms of its radar cross section, σ, with dimensions of area. Assuming this reflected energy expands omnidirectionally, it will be further reduced by a $1/R^2$ factor. The antenna can only collect the fraction of power that hits the dish, so this effective area, A_{eff}, is then multiplied to give the total power received by the radar:

$$P_{\text{rec'd}} = \frac{P_T G A_{\text{eff}} \sigma}{(4\pi)^2 R^4} \tag{2}$$

Based on the electronics and signal-to-noise ratio (SNR) of the radar, if P_{min} is the minimum detectable power, then rearranging (2) to solve for R, we get the maximum theoretical range for the radar to be:

$$R_{\max} = \left(\frac{P_T G A_{\text{eff}} \sigma}{(4\pi)^2 P_{\min}} \right)^{1/4} \tag{3}$$

This range is of course only theoretical. We have not taken into account any atmospheric effects like attenuation or the effect of the shape of the target on scattering. Also, care must be taken to avoid ambiguous range in the returns. If a new pulse is sent out before the round trip time of the maximum range, then the system may consider the return a result of the new pulse and provide a much closer range than exists. Techniques have been developed to avoid this problem [8].

D. RESOLUTION

Good resolution allows a radar system to distinguish one large contact from many smaller contacts (i.e.,. planes flying in formation). If the resolution is high enough, then characteristics on individual planes can be distinguished. The two important resolutions in radar are bearing resolution and range resolution.

1. Bearing Resolution

Bearing resolution is a measure of the minimum discernable angular separation of contacts. It is determined by three factors. First, the beam width and therefore the aperture play a role. Obviously an omnidirectional antenna will provide no bearing resolution at all. The narrower the beam, the better the resolution. Second and third are the rotation rate of the antenna and pulse repetition frequency (PRF). These two must be optimized together. If the antenna rotates more than a beam width between pulses then the radar system will not have complete coverage of the area. It may completely miss a target between pulses. Greater desired ranges mean a slower PRF and therefore a slower rotation rate for complete coverage.

2. Range Resolution

What enables the techniques in this thesis is good range resolution. This is the minimum radial distance between 2 objects that can be differentiated by a single radar pulse. The range resolution will be half the width of the pulse if we think of a simple pulse depicted by the rectangular function in Figure 3.

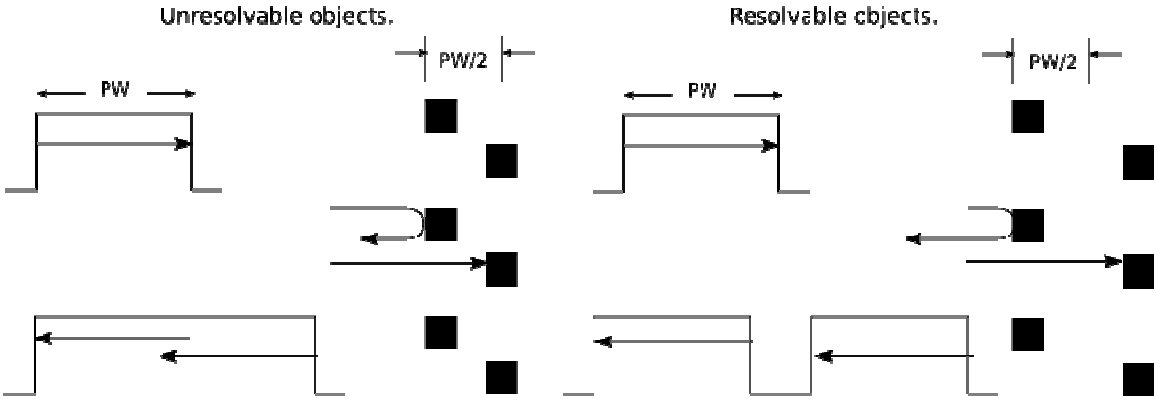

Figure 3. Range resolution using simplified waveform

Much more clever schemes have been derived based on pulse compression and correlation receivers. A common way to achieve greater range resolution is by using more complex waveforms [9]. For instance, instead of using a simple sign wave pulse, a pulse containing changing frequencies can be used. It is called an FM chirp and is depicted in Figure 4.

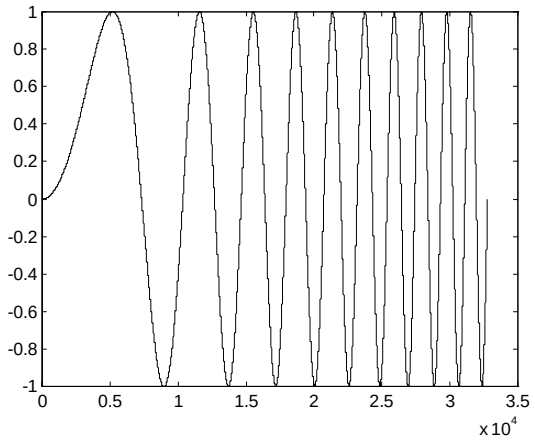

Figure 4. FM chirp representation. [6]

When this non-symmetrical waveform scatters from contacts, the received energy is then correlated with a time and frequency shifted copy of the transmitted waveform. Much closer objects are able to be resolved in this manner. The minimum resolvable separation, ∂r , using this scheme is given by

$$\partial r = \frac{c}{2\Delta f} \tag{4}$$

It is clear that in order to increase the range resolution of these radars, more bandwidth is needed. It is common for bandwidth to be referred to in terms of fractional bandwidth; that is, the fraction of the total bandwidth over the carrier frequency. For instance, a system which operates around 10GHz with a 1GHz bandwidth will have a fractional bandwidth of 10%.

This has been a very brief overview of radar fundamentals and many more considerations exist. The important information applicable to the understanding of the following material has been highlighted. I have discussed how energy is transmitted and received and next we will discuss just what happens when that energy encounters a target, and how that energy is reflected.

III. ELECTROMAGNETIC SCATTERING

I've discussed transmitting energy and waveforms, but what is this energy and how does it propagate? In order to discuss how electromagnetic waves scatter from radar targets, we must first analyze how they get there in the first place. As in most endeavors in electromagnetism, the answer lies in Maxwell's Equations. How do these equations yield the wave equation, and what are the possible solutions? Next, how do these waves interact with the structure of the targets and reflect waves back to the antenna? Lastly, what information can be inferred about the target from the received energy?

A. ELECTROMAGNETIC WAVES

The relationship between fields and charges is described by Maxwell's Equations:

$$\nabla \cdot \vec{D} = \rho_f \qquad \nabla \cdot \vec{E} = 0$$

$$\nabla \cdot \vec{B} = 0 \qquad \nabla \cdot \vec{B} = 0$$

$$\nabla \times \vec{E} = -\frac{\partial \vec{B}}{\partial t} \qquad \nabla \times \vec{E} = -\frac{\partial \vec{B}}{\partial t}$$

$$\nabla \times \vec{H} = \vec{J_f} + \frac{\partial \vec{D}}{\partial t} \qquad \nabla \times \vec{B} = \mu_o \varepsilon_o \frac{\partial \vec{E}}{\partial t}$$

The second set of equations are reached as a result of making a simplifying assumption that we are dealing with a source-free, non-conductive, linear, homogenous, and isotropic medium [10]. These equations are the fundamental equations of electromagnetism and allow us to understand an electromagnetic wave as a time-varying disturbance of the electric and magnetic field which propagates at the speed of light through a medium in a direction perpendicular to each of the fields. A typical representation of the wave is depicted in Figure 5.

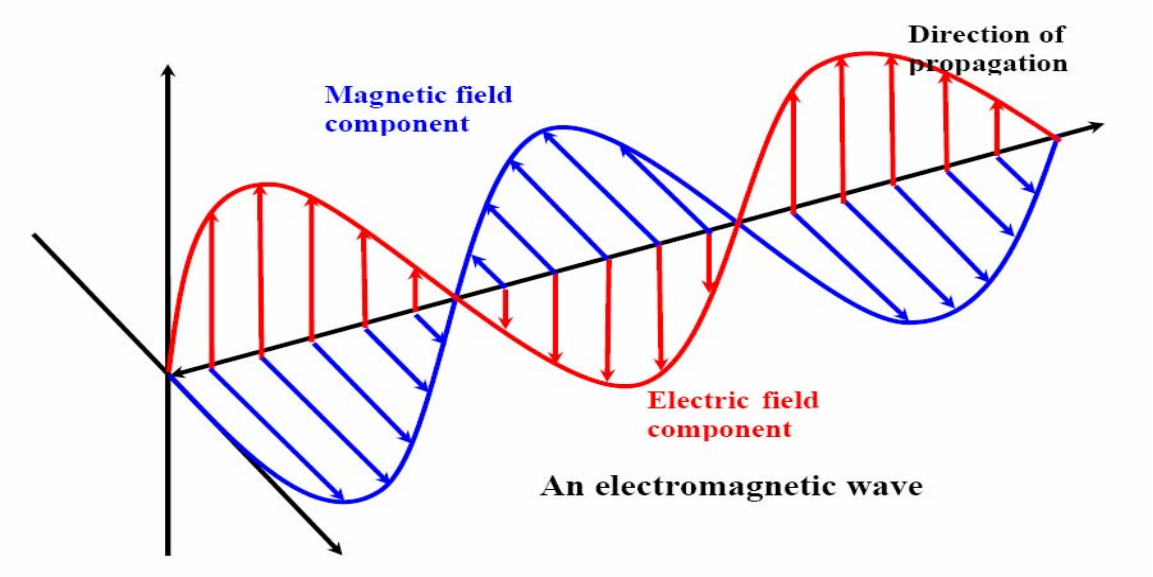

Figure 5. Representation of an Electromagnetic Wave. [11]

If we take the curl of Maxwell's third equation, apply a vector identity, and make substitutions we obtain the vector wave equation

$$\nabla^2 \vec{E} - \mu_o \varepsilon_o \frac{\partial^2 \vec{E}}{\partial t^2} = 0 \tag{5}$$

If we assume that solutions to the wave equation (and Maxwell's equations for that matter) have harmonic time dependence, then the solution can be written in the form

$$\vec{\mathrm{E}}(\vec{x},t) = \vec{E}(\vec{x})e^{-i\omega t} \tag{6}$$

Plugging equation (6) into (5), the wave equation becomes the reduced wave equation, also known as the Helmholtz equation

$$\left(\nabla^2 + k^2\right)\vec{E}(\vec{x}) = 0 \quad \text{where } k = \tfrac{\omega}{c} \text{ and } c = \tfrac{1}{\sqrt{\mu_o \varepsilon_o}} \tag{7}$$

Further simplification of the solution for the wave (6) can be made if we assume that the target is very far away from the source. This is a very good assumption for radar since the target is normally well outside visual range. In this case, the radius of the spherically expanding wave is so great that from the targets perspective, the incoming wave is planar. This approximation allows us to say that the wave has no dependence on coordinates perpendicular to the direction of propagation. The solution can then be written with harmonic spatial and temporal frequencies.

$$\vec{\mathrm{E}}(\vec{x},t) = \vec{E}_o e^{i\left(\vec{k}\cdot\vec{x}-\omega t\right)} \tag{8}$$

This form of a wave is a theoretical abstraction since a perfect plane wave does not exist in nature. For a local frame, far away from the source, it is a reasonable assumption and it will be used to model the incident wave for the scattering discussion in the next section [12].

B. SCATTERING

An electromagnetic wave incident on a conducting surface is a complicated process. Even if we consider a perfectly electrically conducting surface (PEC), to simplify the boundary conditions, the analysis is still mathematically intensive. Although many times it is thought of as the wave 'bouncing' off, this is a misleading perception. In introductory optics, we draw rays hitting mirrors and being redirected as if they're billiard balls on a pool table. Whereas this is a reasonable approximation to make in a high frequency regime, at radar frequencies it does not tell the full story. Upon closer examination, phenomenon such as evanescent waves, skin depth, induced current distributions, and interference are observed. When an electric field reaches a conductor, charges in the conductor are accelerated by the field. We consider a PEC whose charges experience no resistance in motion and can therefore respond immediately to the incident field. These moving charges are a current distribution and therefore also create radiation in the form of a scattered field. Together, the incident field and the scattered field must always satisfy Maxwell's Equations and in turn, the wave equation. The time-independent solutions to the scalar wave equation in spherical coordinates will have the form

$$\Pi_l^m\left(r,\theta,\phi\right) = \frac{1}{\sqrt{kr}} Z_{l+\frac{1}{2}}\left(kr\right) Y_l^m\left(\theta,\phi\right) \tag{9}$$

where Z refers to a Bessel Function and Y to a spherical harmonic. Finding these solutions is very difficult for even the most trivial shapes [13].

Consider the plane wave of equation (8) incident on a PEC sphere. It can be shown that the scattered energy versus wavelength behaves as in Figure 6. In the Rayleigh region, the sphere is much smaller than the wavelength and the scattered energy

is proportional to ω^4. In the Mie region, the sphere and the wavelength are of the same order of magnitude giving rise to resonances as the electrons are accelerated producing constructive and destructive interference. In the optical region, the object is much larger than the wavelength and it becomes more valid to consider the incident wave as rays bouncing off the surface.

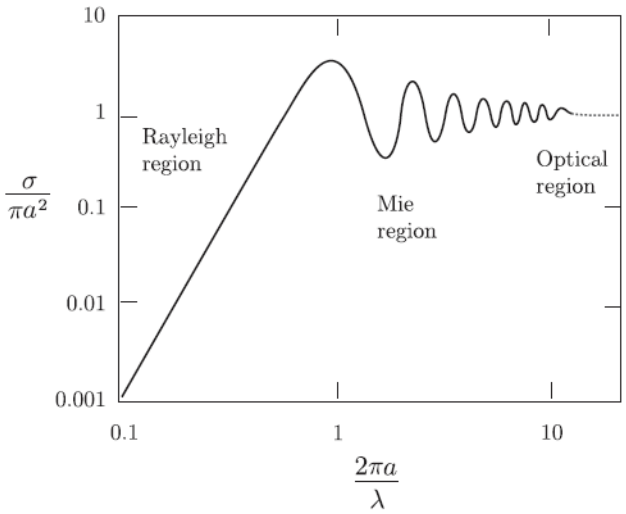

Figure 6. Scattering of a Plane Wave on a PEC Sphere [14].

Since developing analytical solutions to complex scattering geometries is beyond our capabilities, many techniques have been devised to enable automation via a computer to computationally approximate scattered fields from arbitrary objects. Techniques used in the generation of the datasets for this thesis are physical optics (PO) [15], the physical theory of diffraction (PTD) [16], and multiple interactions using shooting and bouncing rays (SBR) [17]. Together, these methods try to approximate scattered fields in a relatively high frequency regime.

1. Physical Optics

The physical optics method calculates the scattered field by relating the incident field to the induced surface currents. This method only considers the initial bounce of the incident wave and not contributions from energy multiply scattered from other parts of the object. This method also does not take into account fringe effects. Since all of the

aircraft models used in the simulations are assumed to be PEC objects, this discussion will also omit the effects of dielectric coatings. If we make what is called the weak scatterer approximation (also known as the first Born approximation), ignoring effects from multiple interactions, then we can write the current distribution as a result of the incident field as

$$\vec{J}\left(\vec{x},t\right) \approx \vec{J}_{po}\left(\vec{x},t\right) = 2\hat{n} \times \vec{H}_{inc}\left(\vec{x},t\right) \tag{10}$$

Using this current density, we can calculate the vector potential $\vec{A}$ and, in turn, the scattered magnetic field. After much algebra, the equation becomes

$$\vec{H}_{scat}\left(\vec{R},t;k\right) = \frac{-ik\vec{H}_o e^{i(2kR-\omega t)}}{2\pi R} \int_{\hat{R}\cdot\hat{n}<0} \hat{R}\cdot\hat{n} e^{i2k\hat{R}\cdot x'} dS' \tag{11}$$

$\hat{R}$ is the direction from the radar to the target and the integral is over the illuminated part of the object. In practice, the target's smooth shape is discretized into hundreds of thousands of small triangles called facets as illustrated in Figure 7. The computer program calculates this integral over each of these flat surfaces and sums the contributions. Representing smooth objects with triangles, of course, introduces error into the calculation, but if modeled carefully with small triangles, this error can be minimized. A ray tracing algorithm is used to ensure only those illuminated facets are included in the calculation.

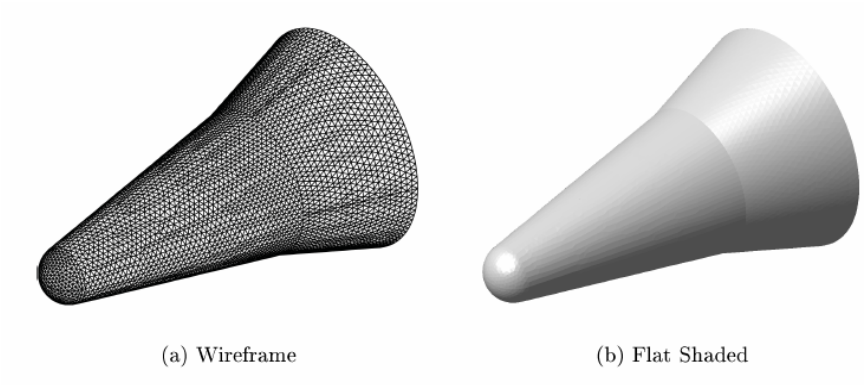

Figure 7. Facetization of a Surface [18]

2. Physical Theory of Diffraction

Physical Optics calculations do not take into account scattering effects due to sharp discontinuities in the geometry of an object. These discontinuities often account for a significant portion of the backscattered energy and should be included in the calculation. Different methods have been devised to deal with these discontinuities including the Geometrical Theory of Diffraction, the Uniform Theory of Diffraction, and the Physical Theory of Diffraction. The computer program used for the simulations here implements the Physical Theory of Diffraction, so that will be the focus of this discussion. Since the geometry files are created from triangles, every intersection of triangles creates an edge. Most of these intersections though are meant to approximate a smooth surface and not a diffracting edge. To ensure that scattering contributions are only calculated from diffracting edges, the angle between adjacent facets is checked and the edge is only used if it's below a predetermined value. In the simulations here, that angle is chosen to be 120^{o}. An illustration of scattering from an edge is given in Figure 8. A set of edges for the geometry is determined and again, only those edges which have incident wave illumination are used in the calculation.

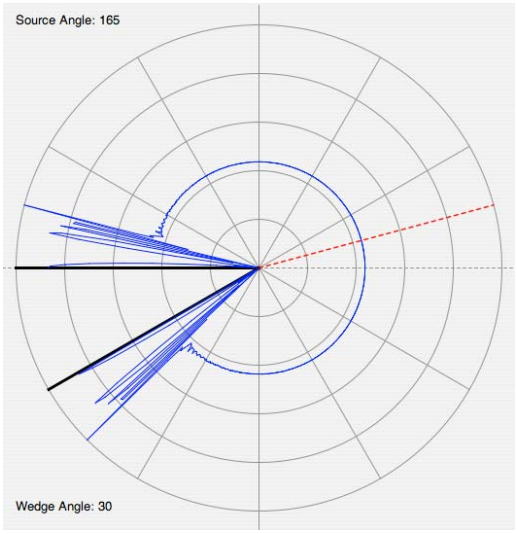

Figure 8. Scattering from a Diffracting Edge [19]

3. Shooting and Bouncing Rays

The two previous methods only took into account the first bounce of the incident wave. After this initial bounce, the scattered waves can then hit other parts of the geometry and rescatter from them. If the electrical size of the target is large, then the bouncing of the waves can be approximated in the high frequency limit. Because the aircraft used in the simulation are much larger than the 3cm wavelengths used in the scattering, bouncing can be approximated using a method called Shooting and Bouncing Rays. Millions of rays spanning each of the different frequencies used are 'shot' at the target. As these rays encounter a facet of the target, they are reflected based on standard geometric techniques. The first facet encountered is ignored as the contribution from the first bounce is calculated with the previous methods. As the ray intersects another facet, the program checks to see if that facet's scattered energy has a line of sight to the receiver. If so, the PO contribution from this facet based on the bouncing ray's orientation is included in the scattered field. The ray then continues its bouncing path until the ray leaves the target geometry and no more bouncing can occur. Each facet that is encountered will contribute to the final scattered field. The limit on number of bounces used in the calculation was set at 20 bounces. In real targets, structures such as jet intakes can allow radar energy to bounce numerous times within the cavity with each bounce contributing to the cross section. Interior structures such as cockpits and engine compartments have limited model detail in the simulation so the detail provided from these structures is only marginally realistic. Interactions between wings, fuselage, weapons, and stabilizers are readily observed. A simplified visual representation of what the computer is actually doing is shown in Figure 9.

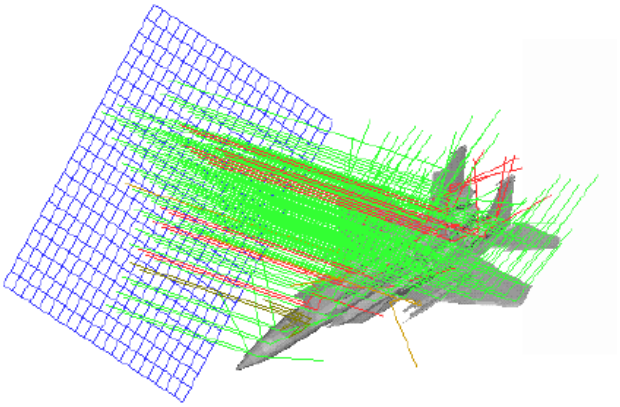

Figure 9. Rays Interacting With F-15 Model [18]

IV. CONTACT IDENTIFICATION

Now that we know how the radar system determines that a contact has been made, the next step is determining what that contact is. The obvious answer of course is to just get on the radio and ask the pilot to identify himself. This method is included in the steps to identify a contact, but there are numerous problems associated with it. Problems include language differences, pilot deception, radio malfunction, operator error, and giving away too much information about the interrogator just by asking the question. The next most obvious answer is to visually look at the contact to determine what it is. This is a reliable method of identification but requires that friendly forces get within visual range of a contact which may or may not be friendly also. Visually identifying contacts becomes a dangerous and time-consuming process with the distances involved. Another rudimentary scheme is identification based on flight profiles. An aircraft flying standard commercial air routes with speeds and altitudes corresponding to a commercial airliner is most likely an airliner. This is of course an easily exploited method that the enemy can use for deception. Automated identification systems which can reach out to the range of the radar provide the best option for early warning of potential hostile contacts and many schemes have been devised and implemented over the years.

A. IDENTIFICATION FRIEND OR FOE

The most widely used and effective system is the Identification Friend or Foe (IFF) system [20]. It is an interrogation and reply based system with 2 channels of communication, one for the question and one for the reply (1.03 GHz and 1.09 GHz). Most air search radars are equipped with a separate antenna to send and receive IFF interrogations and replies. An example of one of these antennas is shown in front of the feed horn of the SPS-49 air search radar in Figure 10.

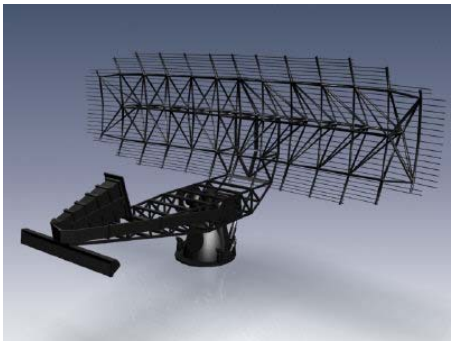

Figure 10. Example of IFF Antenna Attached to the SPS-49 Radar [21]

Multiple modes of IFF are used, each with its own purpose.

- Mode 1 – The mission code used by military aircraft to identify their aircraft type and mission. 64 possible replies.
- Mode 2 – Used to identify the specific tail number of aircraft. There are 4096 possible replies and only military aircraft use this mode.
- Mode 3/A – Mode used internationally for civilian air traffic control and identifies the aircraft's flight number. It can also indicate special circumstances such as emergencies or hijackings.
- Mode 4 – Mode for encrypted military identification. Only with the correct cryptological gear and entered codes can this mode be successfully utilized.
- Mode C – Used for altitude broadcasting to provide air traffic controllers more information on the flight.

IFF provides an efficient means for civilian air traffic controllers to direct planes in the air without having to fill the radio channels with requests for identification. It also gives military users the ability to determine if a contact is a friend. It does not give the ability to reliably distinguish a neutral contact like a civilian airliner from a hostile aircraft. To have effective military use, the current codes must always be entered into the hardware devices. Technician negligence or hardware malfunction make this system of identification less than perfectly reliable. Enemy eavesdropping of successful

interrogations may also allow them to reproduce the transmissions and masquerade as friendly aircraft although advancements in encryption technology significantly reduce this risk.

B. NON-COOPERATIVE TARGET RECOGNITION

When a friend or coworker comes in the room, we know immediately who that person is without having to ask them each time. Also when someone we do not know enters, but is wearing a U.S. Navy uniform, we know that person is probably not an enemy. We understand the identities of these people not by them telling us, but by recognizing features of their bodies, faces, and uniforms. Non-cooperative target recognition (NCTR) serves the same function of trying to identify a contact without asking who they are, and without them telling who they are. The goal is to have sensors like radar be able to tell what a contact is just by 'looking' at it. It is much more difficult for an enemy to change certain structural and mechanical characteristics of their aircraft to try to masquerade as something they are not. Various techniques have been developed to try to extract as much information as possible from the scattered radar energy in order to identify targets.

1. Modulation Schemes

Aircraft are dynamic machines in that they have constantly moving parts. Almost all aircraft have some sort of rotating machinery such as propellers, rotors, or fan blades. These rotating parts can interact with the incident radar pulse causing Doppler shifts at certain modulation frequencies based on the number, size, and rotation rate of the blades. When this principle is applied to aircraft, it is given the names Jet Engine Modulation (JEM), Propeller Rotor Modulation (PROM), and Helicopter Rotor Modulation (HERM) [22]. These signatures, shown as sidebands to the airframe return, can be compared to a library of known signatures to determine its aircraft type. For helicopters, this information is rather constant around the full azimuth range, but for planes, the frequency shifts change depending on azimuth and are most effective from the front or rear of the aircraft. This is a fairly effective method though if the modulation can be picked out of

the noise-laden radar return. The library required for this technique is not that extensive as only engine characteristics need to be stored.

2. Inverse Synthetic Aperture Radar

We often identify things based on pictures and Synthetic Aperture Radar (SAR) is an attempt to use radar waves rather than optical waves to create pictures [5]. Optical devices are able to achieve high resolution because the very small wavelengths used (microns) allow for a very small wavelength-to-aperture (λ/A) ratio. The larger the aperture, the greater the possible cross range resolution. Since radar wavelengths are on the order of cm rather than microns, a much bigger aperture is required to achieve a similar λ/A ratio. By taking multiple discrete measurements while translating the radar, a larger effective aperture can be created. Inverse Synthetic Aperture Radar (ISAR) is mathematically related to SAR via a coordinate shift. The difference is: rather than a fixed object and a moving radar, the radar is stationary and the object is moving. Because of the wavelength size of radar waves, slight changes in range produce large changes of phase in the scattered field. Range must be measured very precisely and range fluctuations must be accurately accounted for. These pictures require some sort of relative rotation rate to acquire the necessary data so there is a time-lag associated with their generation. Once the pictures are created though, identification is as easy as looking at the picture. ISAR techniques are still being perfected and a sample image is shown in Figure 11.

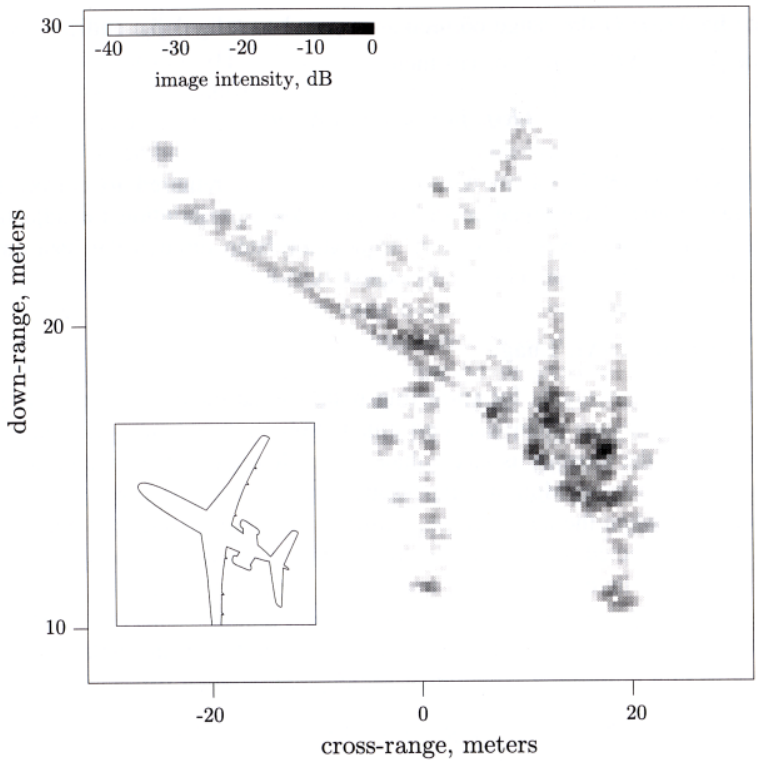

Figure 11. Sample ISAR Image of a Boeing 727 airliner [5]

3. Range Profiles

The high range resolution techniques discussed in Chapter II enable identification methods such as range profiling [23]. Range profiles can be considered one-dimensional images as only down range data is presented with no cross range information. The profile is achieved by taking the inverse Fourier Transform of the frequency domain scattered field measurements. Converting the time domain into the range domain is a simple linear transformation $r = \frac{1}{2}ct$. The greater the bandwidth of the receiver, the better the resolution in the range profile.

A range profile shows peaks at the major scattering centers of the aircraft. The distance between peaks corresponds to the radial (range) distance between the centers. As the target angle of the aircraft changes, different parts of the aircraft will come in to illumination and change relative positions on the range profile. This means that a range profile can change significantly as the target rotates. Also, the multiple scattering

mechanisms that were discussed in Chapter III will cause peaks to show up in the range profile that do not correspond to a line of sight range, but rather the sum of the paths of the bounces. Also, parts of the aircraft will scatter strongly at some angles, and weakly at others. For instance, the wings of the aircraft may couple nicely with a horizontally polarized radar pulse where the vertical stabilizers will not. Conversely, if the aircraft banks 90 degrees, the stabilizers will be more effective scatterers and may show up strongly. A sample range profile of a model F/A-18 used later in the simulation is shown in Figure 12.

The process of identification based on range profiles is a similar process to the modulation schemes previously discussed. A library of range profiles must be compared to the sampled profile, and which ever profile more closely matches is the likely identity. A library must include every aircraft expected to be encountered or the search will obviously report an incorrect match. Also, depending on the resolution of the system and how rotationally sensitive the profiles are, the library will have to have profiles covering fractions of degrees for every possible combination of azimuth and elevation. Another factor is that many aircraft are not configured the same for every flight. Some flights require external fuel tanks, bombs, missiles, etc. These extra features can significantly alter the range profile and they must also be taken into account in building the library. The libraries can be built with actual model aircraft on a range or with computer generated models and radar cross section estimation tools such as the ones used in the simulation. With all these factors to consider, obviously building dense enough libraries to reliably identify contacts will take millions of stored profiles. Searching the library must also be done in a reasonable amount of time (a few seconds) or the information won't be actionable.

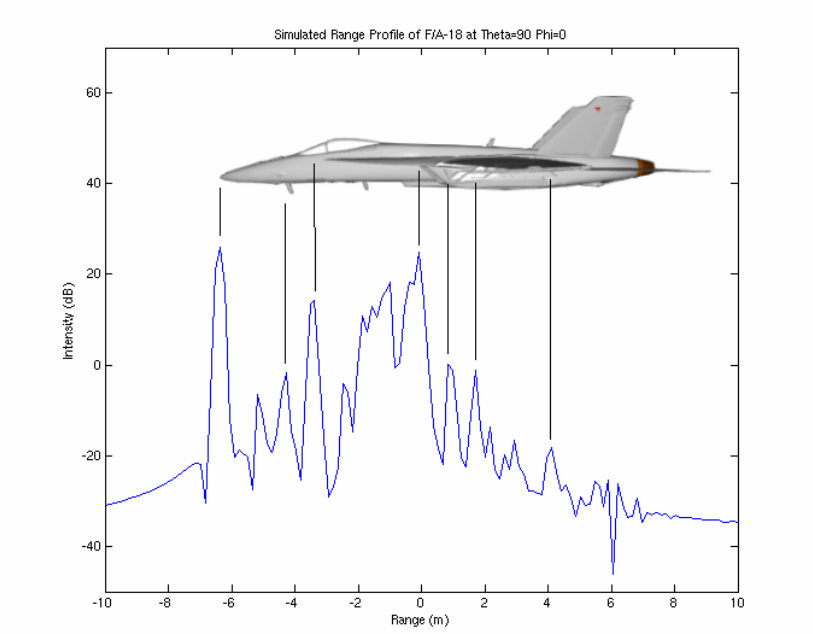

Figure 12. Simulated Range Profile of an F/A-18

4. Bispectrum Profiles

Range profiles contain scattering information for not just the first bounce, but for multiple bounces also. The information is depicted in the same manner though and it is almost impossible to visually separate the first bounce peaks from the multi-bounce peaks. Creating what are called bispectrum[1] images can help in identifying the multiple interactions of a target by separating them from the other terms [24]-[28]. The idea is that different aircraft types will have different characteristic interactions between the structures on the airframe. If these interactions can be isolated by the bispectrum, then a more informed comparison can be made with a library of signatures.

The bispectrum is defined as the two-dimensional Fourier transform of the third order cumulant function of the scattered field measurements and is given by the following equation in the time domain where $h(t)$ is the impulse response of the target:

$$B(t_1, t_2) = h(t_1)h(t_2)h^*(t_1 + t_2) \tag{12}$$

[1] Also called *birange* or *bitime*, depending on the domain. I will use the term *bispectrum* to refer to this class of images.

The bispectrum therefore will have a strong peak wherever two peaks in the range profile can be associated with a peak further down in the profile. This indicates a possible interaction between these two scatterers. As each aircraft will have different interactions, these spots will show up at different places in the bispectrum, and a library can be searched in the same manner as before. It has been suggested that the bispectrum of a target has more rotational invariance than a range profile and therefore the library can be sparser. Bispectra also have the ability to suppress Gaussian white noise and therefore may be more useful in noisy environments than range profiles which do not suppress noise.

C. 3 POINT SCATTERERS EXAMPLE

In order to illustrate the previous two methods, consider a simple widely used example – 3 point scatterers in space. It was presented in a previous thesis on the topic by Jiunn Wah Yeo [11]. The setup of the example is shown in Figure 13.

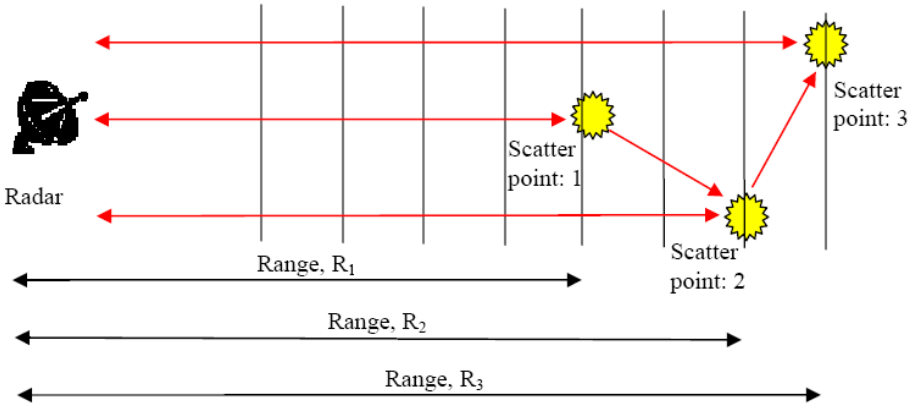

Figure 13. Illustration of 3 Point Scatterers Example [11]

Yeo shows that when $R_1 = 0$m, $R_2 = 1.5$m, and $R_3 = 3.6$m, the scattered field can be reduced to

$$H(f) = C_1 + C_2 e^{-i\left[4\pi(1.5)\frac{f}{c}\right]} + C_3 e^{-i\left[4\pi(3.6)\frac{f}{c}\right]} + C_4 e^{-i\left[4\pi(5.1)\frac{f}{c}\right]} \quad (13)$$

where $C_{1,2,3,4}$ are constants. The Fourier transform of this signal will provide the range profile of these 3 point scatterers shown in Figure 14. The first 3 peaks correspond to the positions of the 3 points, but the 4th peak, noted as a "ghost" artifact, is due to the multiple scattering between the 3 points.

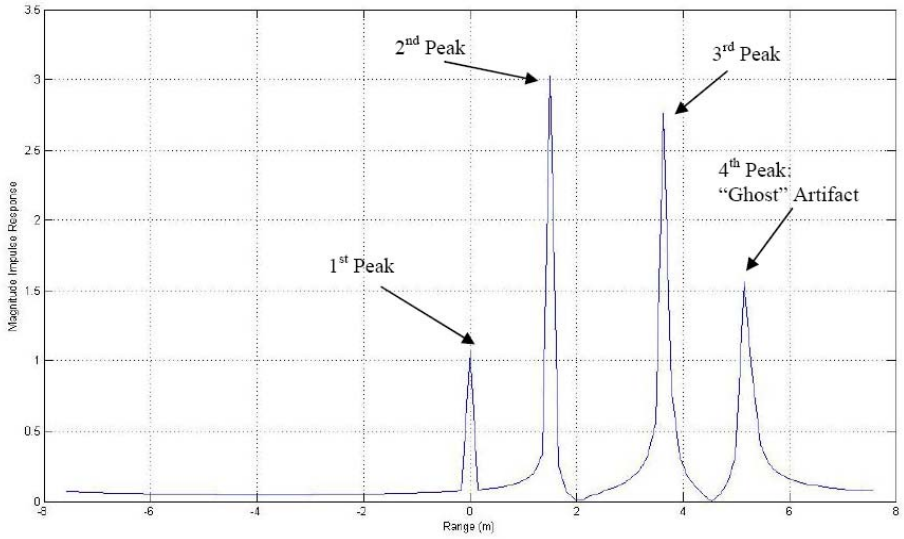

Figure 14. Range Profile of 3 Point Scatterers [11]

A bispectrum plot can be created from the same frequency signal and is shown in Figure 15. In this image, the strong peaks indicate interactions by the second and third point. We also notice the symmetry properties of the bispectral image. A diagonal line through the origin in this particular image is the symmetry axis. A more complex target will naturally provide for more interactions and we will notice in the simulation, that much more complex bispectrum images are created by aircraft targets.

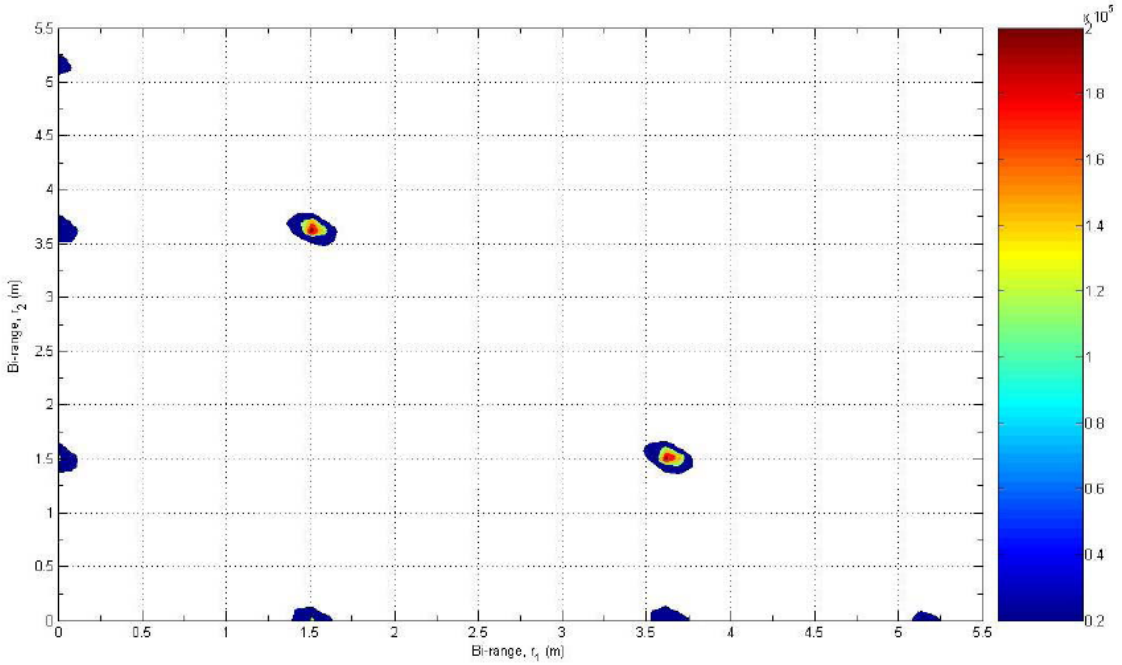

Figure 15. Characteristic Bispectrum Plot of 3 point Scatterers [11]

V. SIMULATION

The goal of this thesis is to determine whether a classification system based on bispectrum images is a valuable enhancement or substitute for a system using range profiles. Since both systems need a library of aircraft signatures with which to compare, an experimental library had to be created. Afterwards, 4 sets of test cases were created and identifications of these test cases were made based on the two methods. A comparison of the simulation results follows in Chapter VI.

A. BUILDING THE LIBRARY

1. Scenario

Since I'm not concerned with actually building a fieldable system and, instead, only with a performance comparison between algorithms, I do not need to have a library of every possible aircraft, configuration, and aspect angle. I begin with considering the situation I want to model. The most useful scenario for an early warning identification system is when a ship or aircraft detects an incoming contact at a distant range. Is the contact a potentially hostile enemy fighter, or is the contact a neutral commercial airliner? The sooner this question can be answered, the more likely we will be able to avoid another Vincennes-type disaster. This scenario is depicted in Figure 16.

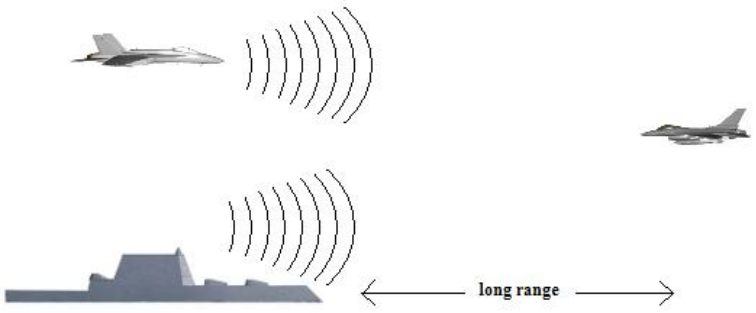

Figure 16. Simulation Scenario

2. Aircraft

A real library of radar signatures should include every aircraft type that can be expected to be encountered on the mission. To build my test library, I included 10 aircraft from a collection that would be similar enough to test the recognition methods, but also a few outside the class to provide a reality check. I chose eight fighter/attack aircraft, one helicopter, and one commercial airliner. The aircraft are from a collection of commercial 3-D models from a company called Mesh Factory [29]. The aircraft's smooth surfaces are constructed from individual triangles and these triangles are what enable the use of the scattering techniques described in Chapter III. For instance, the F/A-18E Super Hornet, constructed from over 83,000 triangles, is depicted in Figure 17.

Figure 17. Model and Wireframe of F/A-18E Super Hornet

Fighter aircraft do not fly every mission with the same configuration. Some missions require external fuel tanks and an assortment of bombs, while others require only air-to-air missiles. In order to test the abilities of these methods to deal with alternate configurations, each of the fighter aircraft were also given a set of appropriate munitions for an additional test set, a 'dirty' test set. These additional configurations were not included in the library, only the test cases. The position of the helicopter's main

rotor was also changed because every radar pulse on a helicopter will encounter the blades in a slightly different aspect allowing different scattering interactions. The Airbus A320 was not reconfigured as no external weapons seemed appropriate for the airframe. Appendix A provides a visual depiction of the aircraft and configurations used.

3. Aspect Angles

There is, of course, a performance/time trade-off between having a library dense enough to guarantee accurate identification, and a library sparse enough to be able to search through very quickly. In order to limit the size of the library, I first make the assumption that the aircraft are symmetric about the centerline – that is, that their port side is the same as their starboard side. This is not true of real aircraft as different munitions may be attached to each side and sensors may be attached anti-symmetrically. I neglect these effects for simplicity. A spherical coordinate system is used rather than the azimuth/elevation system. Because I am considering incoming contacts, I chose a range of target angles that would cover the expected vantage points. The angles are depicted in Figure 18. Each aircraft was scaled so that its wingspan is equivalent to the actual aircraft's wingspan in meters.

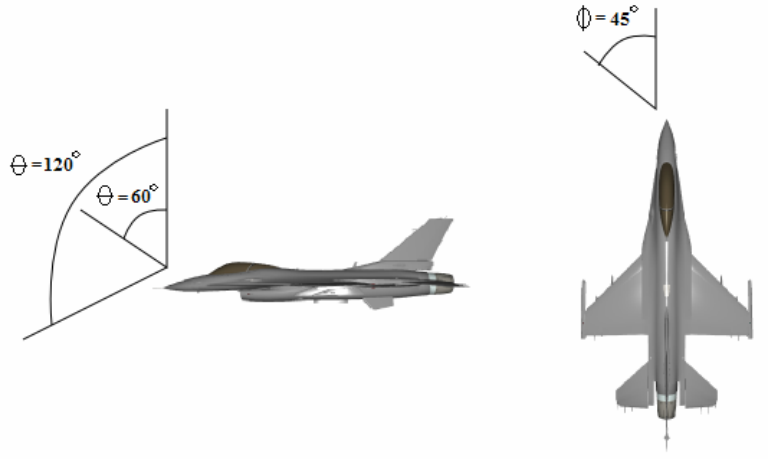

Figure 18. Range of Angles Considered

I gathered radar data for angles from 60° below vertical to 120° below vertical in 5° increments, and from 0° ahead to 45° to port (315° relative) in 3° increments (which, in

effect, covers from +45^{o} to -45^{o} due to symmetry). These angle combinations give 208 profiles per aircraft providing a total library of 2080 searchable profiles. Admittedly this is a rather sparse library for extremely accurate identification, but it provides the means to compare the performance of the two methods side-by-side.

4. Radars

I consider radar contact acquisitions from aircraft radar and from shipboard radar to compare the differences in the performance of these methods at different frequencies and bandwidths. In order to ensure that this simulation remains unclassified and freely distributable, actual radar system specifications were not used. For the aircraft radar I simulate an X-band radar with 1 GHz bandwidth centered at 9.5 GHz. Using this bandwidth in equation (4) gives a range resolution of 15cm. For the shipboard radar I simulate a C-S band radar with a 400 MHz bandwidth centered at 4 GHz. This bandwidth provides a range resolution of 37.5cm. A separate library for each radar was built with the different scattering signatures.

5. RCS Tools

The radar cross section (RCS) estimation tool used to create the library is a program called Lucernhammer from Tripoint Industries [18]. It takes as input a facet file containing the aircraft geometries and calculates the scattered field using the PO, PTD, and SBR techniques described in Chapter III. The ability to model materials with different reflectivity and dielectric coefficients exists, but was not employed. The facet files are considered complete PEC objects which introduces inaccuracies in the signatures, but is satisfactory for comparison between the two methods. It generates a file containing the complex-valued scattered field measurements for each combination of θ and ϕ used for the library. The data are normalized so that the square of the magnitude is the radar cross section in square meters. 256 sampling points were taken within each bandwidth range allowing the range profiles to include the entire physical range of the aircraft models. The models were scaled to the appropriate dimensions mentioned before so that the wavelength relative to structure would be realistic. Lucernhammer has the ability to calculate scattered field in multiple polarizations, but the

horizontally transmitted and horizontally received polarization was chosen for the simulation. A special purpose file conversion utility was written to extract the desired information from the scattered field file and organize it into a Matlab friendly structure.

6. Processing of Frequency Domain Data

The frequency domain scattered field files were loaded into Matlab and separated into individual cell arrays. Each frequency array was normalized for unit energy. Range profiles were generated by applying the inverse Fourier transform to the simple rectangular windowed data. These range profiles cover a range of +/- 19.112 m and are 256x1 arrays of complex-valued data. A library of bispectrum data was also generated using the code adapted from [11] in Appendix C. Each bispectrum is a 511x511 array of complex-valued data.

B. RUNNING THE SIMULATION

1. Test Cases

The likelihood of trying to compare a test signal that is exactly the same as something in the library is practically non-existent. A radar return, especially from a distant target, is full of noise at different levels. Also, the aircraft will have slightly different configurations and will be a different aspect angles than what is in the library. I do not consider the effects of noise in the simulation. Since I was working with a rather sparse library, I was able to compare classifications at angles very near library angles and further away. My first data set was generated using the same aircraft configurations I used in building the library. I looked at combinations of angles 1 to 2 degrees away from library angles. I took data from each aircraft at 5 angle combinations spread across the library range and repeated those same combinations for each aircraft giving 50 total test cases for the first set. The second set is using the same aircraft configurations as the first, but with closer angle combinations within 1 degree of the library angles. 50 additional test cases were generated for this set. The purpose of these two sets is to compare the rotation invariance of the two identification methods and to see which method is degraded more by having a sparse library.

For the second two test case sets, the armed aircraft configurations described in Section V.A.2 were used. The first set includes exact angle combinations that are found in the library. Since noise was not added to the simulation, both methods would locate an exact replica of a library signal 100% of the time. Changing the configuration of the aircraft alone enables an analysis of the ability of the two methods to handle alternate configurations. 45 test cases for this set were created because the A320 was not reconfigured. The next set of test cases again use the armed configurations, but this time use the same close offset angles that were used in the second set of the stock configurations. In this set, the ability to handle both offset angles and multiple configurations is tested. Additionally, a direct comparison can be made with the second stock set to further determine how much configuration changes impact the identification methods.

2. Range Profile Correlation

At the heart of the range profile based simulation is the question of how to determine which library entry most closely matches the test case. Because the profiles were all created from similarly normalized frequency data, they can be compared directly. The method of comparison used is the cross-correlation [5]. The correlation coefficient is the measure of how closely the two match and is given by the equation

$$C(n,\theta,\phi) = \max_{y\in\Re} \int_{\Re} p_{test}(y')\, p_n(y'+y;\theta;\phi)dy' \tag{14}$$

where n is the type of aircraft and θ and ϕ provide the aspect. The Cauchy-Schwartz inequality tells us that $C(n,\theta,\phi) \le 1$. It equals one when the two signals are exactly alike (within a translation). The correlation giving the highest coefficient is selected as the identification and the likely aspect of the target is also extracted. The cross correlation is implemented in the simulation within the howCorrP.m file in Appendix C. It takes two complex range profiles and returns the correlation coefficient of the two. Matlab's xcorr function is used with the magnitudes of the two signals.

3. Bispectrum Correlation

The bispectrum based simulation also uses the idea of the cross-correlation but implements it differently [28]. Because the bispectrum profiles are 2-dimensional arrays, a 2 dimensional cross correlation must be used. The time or range domain based xcorr2 function in Matlab would take an unreasonable amount of time to complete, so the correlation is done in the frequency domain. The equation used is

$$\rho_{t,n}(r_1, r_2) = \frac{ifft2\left\{R_t(f_1, f_2)R_n^*(f_1, f_2)\right\}}{\left[\sum_{f_1}\sum_{f_2}\left|R_t(f_1, f_2)\right|^2\right]^{1/2}\left[\sum_{f_1}\sum_{f_2}\left|R_n(f_1, f_2)\right|^2\right]^{1/2}} \tag{15}$$

R in this equation is the two-dimensional Fourier transform of the magnitude of the bispectrum profile. The correlation coefficient is extracted by taking the maximum value of this 2-D array over r_1 and r_2. The implementation of this correlation can be found in the file howCorrBi.m in Appendix C. It takes as input the Fourier transform of two bispectrums and returns the correlation coefficient. Once again the identification is selected as the comparison with the highest correlation coefficient.

4. Program Flow

The correlation simulations operate by comparing each test case with every signature in the library and combining the results. The maximum overall correlation for each test case is designated the identification and noted in the output file. A matrix containing the tally for each identification versus test case group is also created. Test cases involving different aspects of the same aircraft are summed or averaged together. In addition to determining the maximum correlation for each test case, the simulation determines how closely each test case correlates to each aircraft type by filling an array with the maximum coefficient of correlating the test case with aircraft type. These 1x10 arrays of coefficients for each test case are grouped again by test type and averaged to simulate the performance of averaging multiple radar hits together for increased identification accuracy. Simulation code is given in Appendix D and program flow logic flow is given below.

```
for each set of test cases
        load test case set
        open output file
        for each test case
                check test case with entire library
                make array out of all correlations
                find maximum correlation
                        designate it the identification
                find maximum of subarrays
                        add to coefficient matrix
                write identification to output file
        end for
        average coefficient matrix
        write matrices to output file
end for
```

VI. ANALYSIS

A. SIDE BY SIDE COMPARISON

The similarities of the bispectrum plot and the range profile are evident when we look at them side by side with the same range scale as shown in Figure 19. The contour plot depiction of the bispectrum shows the highest peaks as red and lower points as blue. If we look at a horizontal line across the bispectrum at $Range_y=0$, we see that the spikes in the range profile closely correspond to the peaks of the bispectrum.

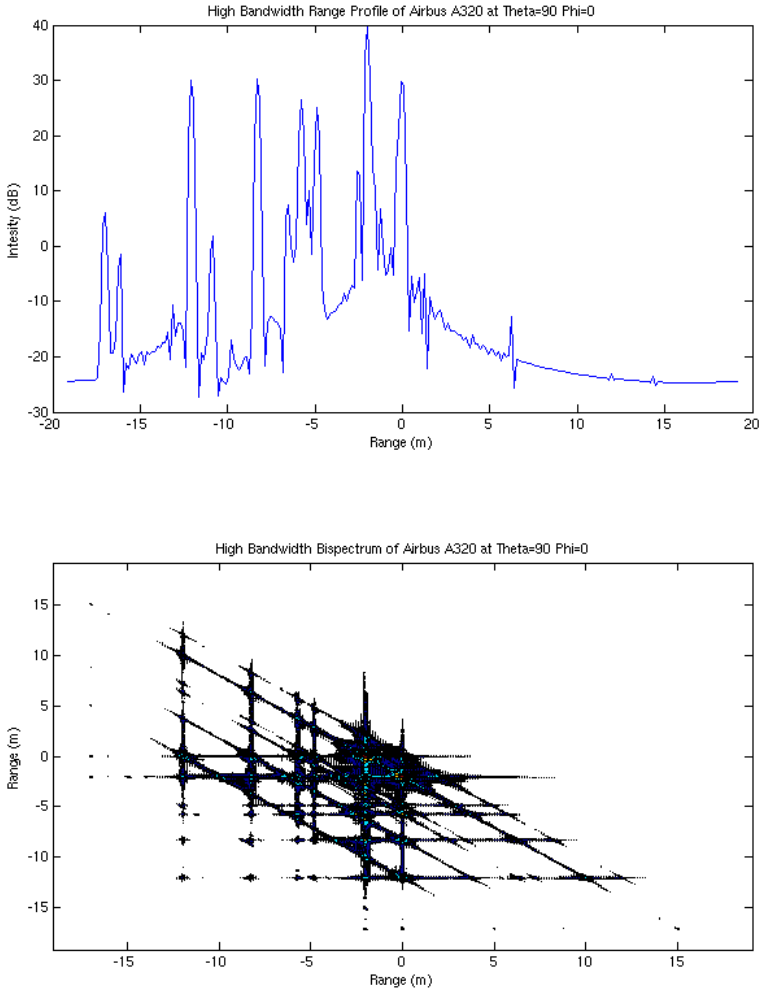

Figure 19. Range Profile and Bispectrum Plot of A320

Comparing the range profile to the aircraft we see that the peak at a range of -12m likely corresponds to returns from the engine intake. If we look at a horizontal line (or vertical due to symmetry) at a range of -12m, we see many other peaks down the line. These peaks indicate that the scattered energy from the engine interacts with many structures down range — likewise with other structures.

B. THE EFFECT OF BANDWIDTH

As shown earlier, greater bandwidth allows greater range resolution. When trying to distinguish small fighter aircraft from one another, good range resolution is very important. The level of range profile detail lost from a front aspect view of an F-15 when we go from 1GHz bandwidth high frequency radar to the 400MHz bandwidth lower frequency radar is shown in Figure 20. The range resolution in the latter is not good enough to distinguish between parts of the aircraft very near others.

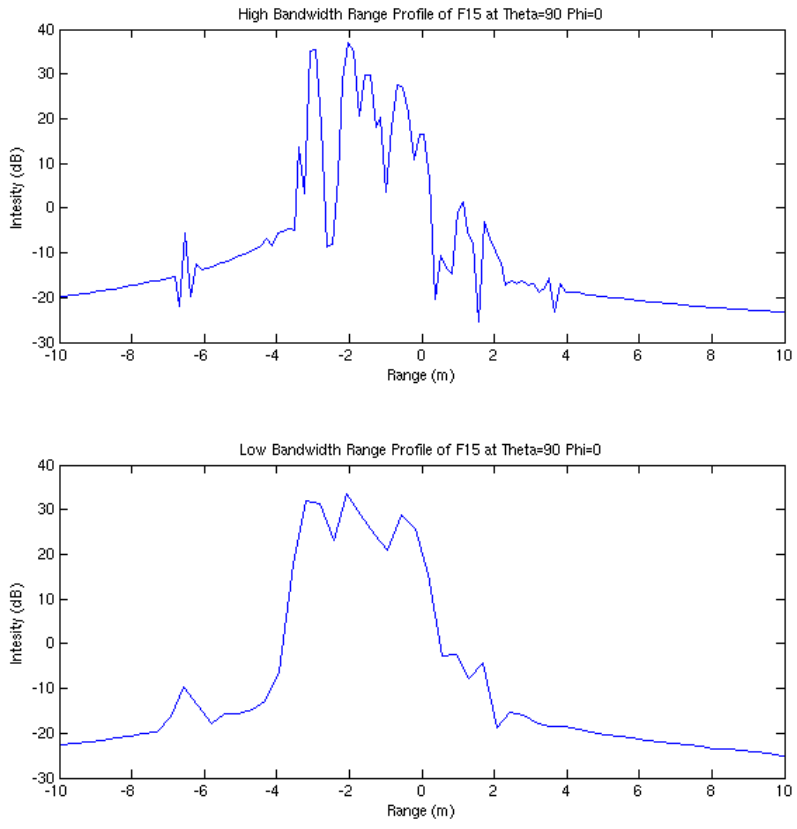

Figure 20. Range Profiles of F-15E at HBW and LBW

Fewer features are present to enable us to distinguish the airplane from other similar fighters and we will see how this limitation will impact the classification programs. Just as the lack of bandwidth decreases the fidelity of the range profile, it also impacts the bispectrum plot. The difference in bispectrum plots of the same F-15 at the two bandwidths is shown in Figure 21. The tight peaks of the multiple interactions of the high bandwidth plot are much wider in the low bandwidth plot. The lower fidelity of the low bandwidth bispectrum plots will enable greater correlations with slightly different plots, and should cause classification errors.

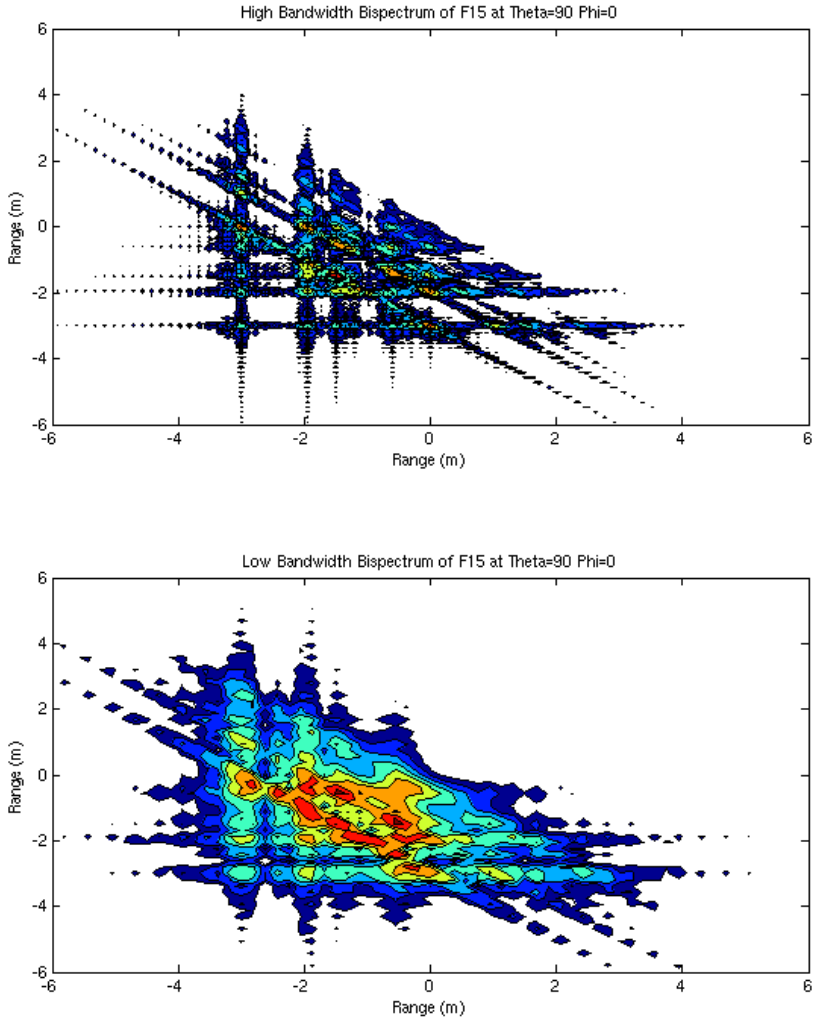

Figure 21. Bispectrum Plots of F-15E at HBW and LBW

C. ROTATIONAL VARIANCE

Slight rotations of the aircraft can significantly change the scattered field. The sharpness of the high bandwidth plots shows this effect very clearly. The difference in the range profile of an F/A-18E from $\theta = 95^{o}$ as we rotate from $\phi = 21^{o}$ to 27^{o} is shown in Figure 22. We see how the many scattering points of the engines and weapon pylons interact and change with a small rotation. This sensitivity highlights the importance of having a library with very close angles and the simulation will further illustrate this.

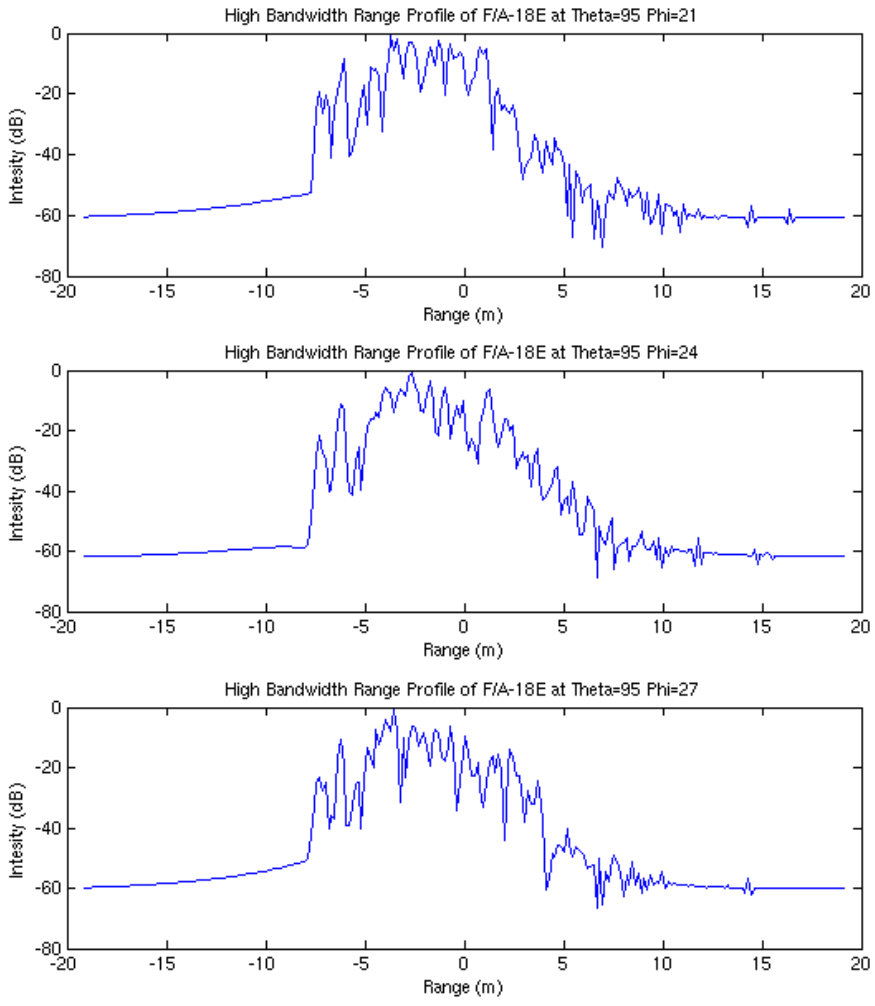

Figure 22. Rotational Variance of F/A-18E Range Profiles

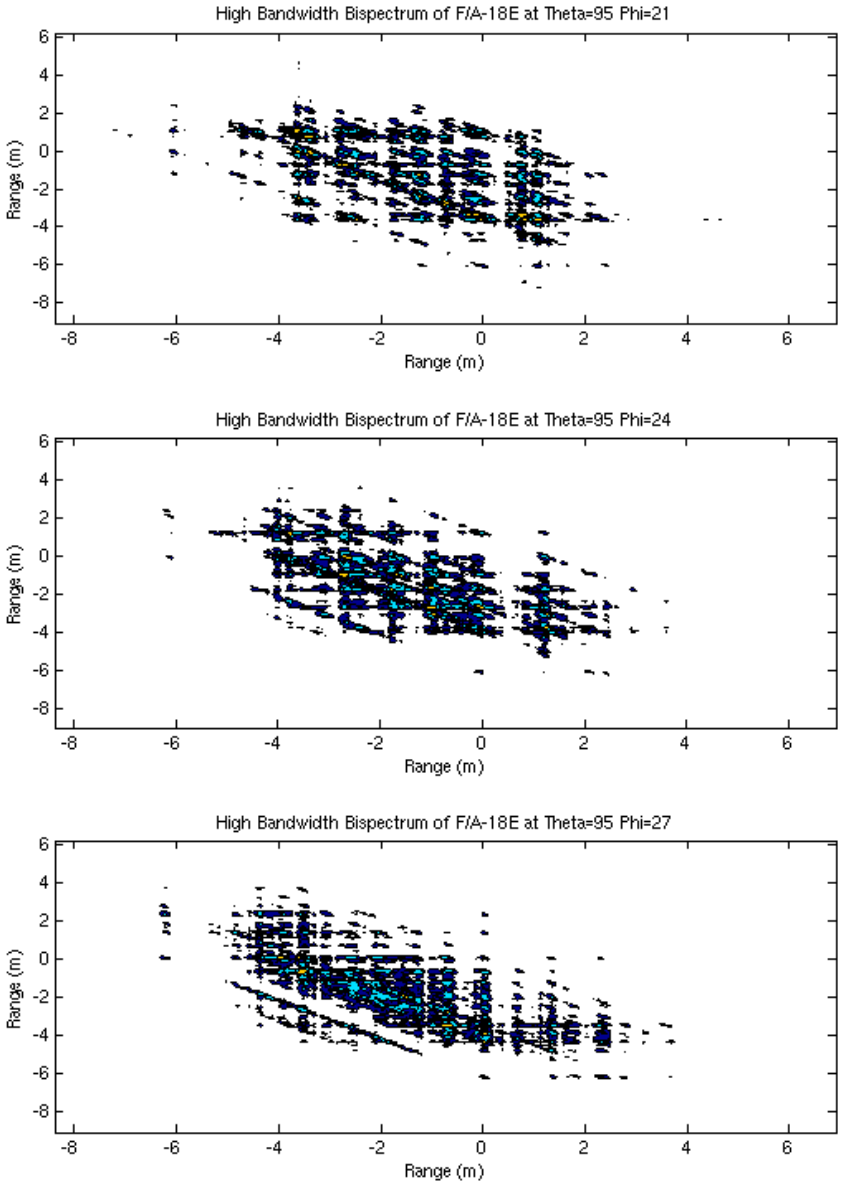

Figure 23. Rotational Variance of F/A-18E Bispectrum Plots

The same F/A-18 aspect and rotation is shown in Figure 23. We see that even with the bispectrum, the plots change significantly. The radar wave bouncing from structure to structure is very sensitive to incident angle. By the time the aircraft rotates the full 6^{o}, the plot looks very dissimilar to the original. Tables 1-4 show this effect with correlation coefficients. The model F/A-18E at $\theta = 95^{o}$ and $\phi = 21^{o}$ was correlated with its neighbors using range profiles and bispectrums at different bandwidths. The profile

correlations at each bandwidth returned similar results and we note that the rotation does not change the range profile correlation by a large percentage. This may cause problems when trying to classify similar targets. The bispectrum correlations show that the test case did not correlate well with its neighbors. A large percentage change in the correlation coefficient is returned when the contact is rotated by a few degrees. We also note that the low bandwidth provided less of a difference than the high bandwidth as expected. This large difference in rotational similarity should not make the bispectrum able to handle large angle disparity.

		Phi		
		21	24	27
Theta	95	1.0000	0.7254	0.8233
	100	0.8300	0.7995	0.7933
	105	0.7170	0.7194	0.7499

Table 1. Rotational High Bandwidth Profile Correlations

		Phi		
		21	24	27
Theta	95	1.0000	0.8746	0.8000
	100	0.8279	0.7783	0.8169
	105	0.8113	0.8271	0.7749

Table 2. Rotational Low Bandwidth Profile Correlations

		Phi		
		21	24	27
Theta	95	1.0000	0.0859	0.1236
	100	0.0991	0.0783	0.1157
	105	0.0880	0.0940	0.0934

Table 3. Rotational High Bandwidth Bispectrum Correlations

		Phi		
		21	24	27
Theta	95	1.0000	0.1944	0.1480
	100	0.2282	0.1848	0.1612
	105	0.1618	0.1766	0.1257

Table 4. Rotational Low Bandwidth Bispectrum Correlations

D. CONFIGURATION CHANGES

A change in the configuration of an aircraft has a great effect on the range profile and bispectrum. External fuel tanks, missiles, and bombs can contribute a large portion of the backscattered signal. The difference in the range profile of an unarmed F-16 with $\theta = 120^{o}$ and $\phi = 45^{o}$ and the armed version at the same aspect is shown in Figure 24. The additional structures cause peaks to appear in the profile where none exist in the unarmed profile. The bispectrum plots of the same aircraft are shown in Figure 25. We see that not only do new scattering interactions appear, but interactions present in the unarmed plot disappear. This can be due to masking of structures by the armaments or interference of the free path of the waves.

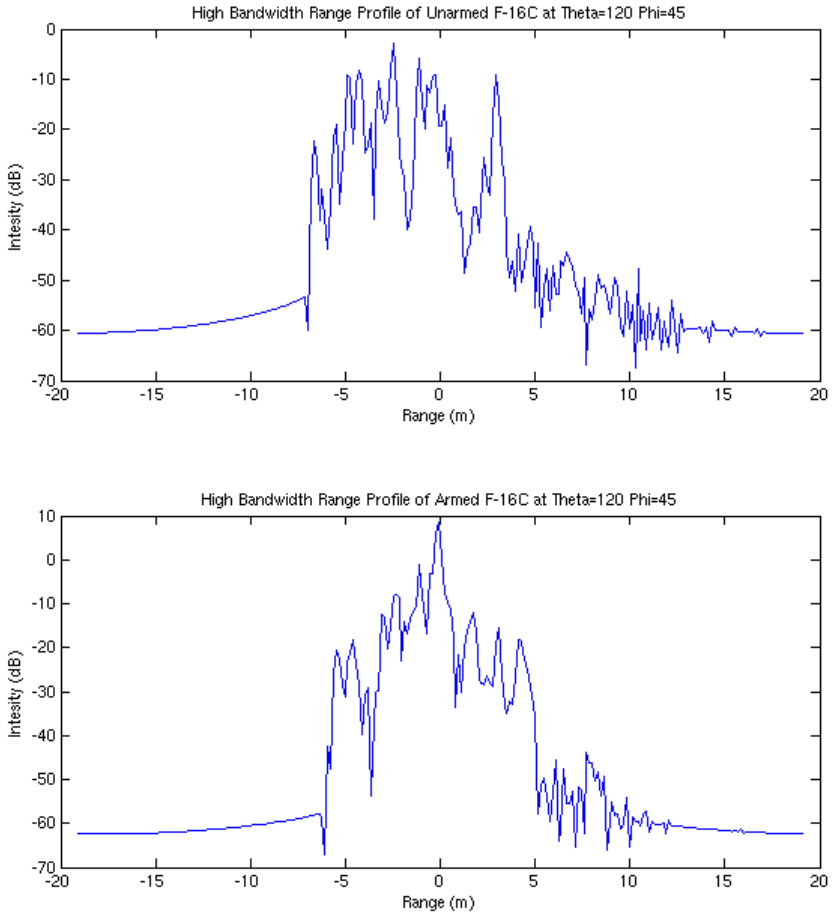

Figure 24. Multi-Configuration Range Profiles of F-16C

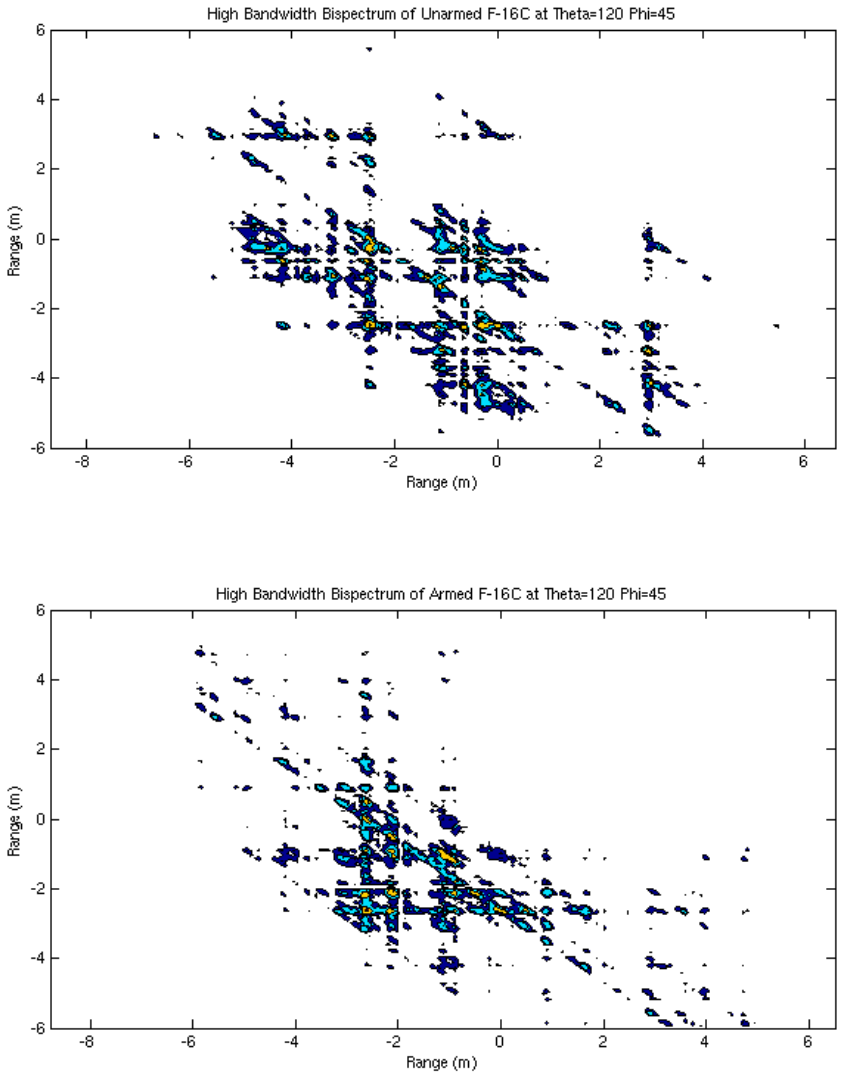

Figure 25. Multi-Configuration Bispectrum Plots of F-16C

E. SIMULATION RESULTS

The results of the simulations described in Chapter V are analyzed by section below. The individual results are provided in Appendix E.

1. High Bandwidth Results

The high bandwidth (HBW) range profile simulations involving the stock aircraft showed promising results. Based on individual test cases, the success rate was only 60%

per set, but when multiple radar hits of the same test aircraft were averaged together, the highest correlation coefficient corresponded to the correct aircraft every time. The highlighted block in the tables indicate the maximum coefficient in each row. There is not much margin for error though as the coefficients all range between 0.75 and 0.90. The hypothesis before the tests were run was that the second set, with angles very near the library angles, would show a greater correlation than the first set. Tables 5 and 6 show that hypothesis was incorrect for the range profiles – it was true for only 5 of the aircraft and the coefficients had a similar range in each table.

Test Cases \ Library Aircraft	A320	EA6B	F4	F14	F15	F16	FA18	MiG	Su27	UH60
A320	0.8434	0.7883	0.8048	0.7966	0.7877	0.7933	0.7861	0.7828	0.8037	0.7871
EA6B	0.8158	0.8474	0.8013	0.7887	0.7988	0.8002	0.8052	0.7908	0.8064	0.7987
F4	0.8040	0.8196	0.8693	0.8215	0.8426	0.8481	0.8482	0.8398	0.8200	0.8455
F14	0.7741	0.8347	0.8344	0.8618	0.8142	0.8331	0.8346	0.8253	0.8171	0.7937
F15	0.8364	0.8327	0.8631	0.8408	0.8777	0.8559	0.8670	0.8462	0.8449	0.8486
F16	0.7882	0.8112	0.8355	0.8423	0.8188	0.8712	0.8343	0.8139	0.8323	0.8311
FA18	0.8510	0.8482	0.8703	0.8697	0.8706	0.8703	0.8816	0.8616	0.8630	0.8707
MiG29	0.7621	0.8048	0.8384	0.8028	0.8153	0.8155	0.8199	0.8541	0.7947	0.7992
Su27	0.7838	0.8181	0.8201	0.8263	0.8225	0.8222	0.8164	0.8142	0.8426	0.7825
UH60	0.8222	0.8118	0.8559	0.8073	0.8262	0.8388	0.8410	0.8151	0.7982	0.8792

Table 5. HBW Range Profile Simulation With Stock Aircraft at Far Angles

Test Cases \ Library Aircraft	A320	EA6B	F4	F14	F15	F16	FA18	MiG	Su27	UH60
A320	0.8676	0.8148	0.7992	0.8157	0.8169	0.8172	0.7896	0.7947	0.7942	0.8187
EA6B	0.7417	0.8554	0.7627	0.7720	0.7774	0.7807	0.7773	0.7908	0.8041	0.7425
F4	0.7919	0.8065	0.8891	0.8337	0.8402	0.8320	0.8434	0.8450	0.8125	0.8209
F14	0.7934	0.8280	0.8232	0.8468	0.8191	0.8241	0.8331	0.8187	0.8144	0.8178
F15	0.7574	0.7845	0.7907	0.7887	0.8467	0.7757	0.8022	0.8029	0.7903	0.7746
F16	0.7949	0.8092	0.8099	0.8310	0.8217	0.8619	0.8213	0.8140	0.8125	0.8253
FA18	0.8061	0.8161	0.8283	0.8147	0.8195	0.8447	0.8539	0.8102	0.8188	0.8275
MiG29	0.7533	0.8193	0.8284	0.8165	0.8206	0.8261	0.8091	0.8498	0.8093	0.7813
Su27	0.7535	0.7902	0.7853	0.8046	0.7830	0.7742	0.7937	0.7904	0.8466	0.7720
UH60	0.8331	0.8470	0.8779	0.8427	0.8607	0.8845	0.8730	0.8369	0.8388	0.8950

Table 6. HBW Range Profile Simulation With Stock Aircraft at Near Angles

The same two test sets run with the bispectrum algorithm produce different results. There was a 58% individual success rate for the first set and an 80% success rate for the second set with closer angles. Because the HBW bispectrum plots produce such narrow peaks, the plots are more easily misaligned and the correlation coefficients are in the .4-.7 range. What is important is the difference between the maximum coefficient and the others in the row. After averaging the test cases, the simulation misidentified the A320 as an EA6B in the first set of tests. The rest of the test cases were correctly identified after averaging. Because of the greater individual success rate and the greater difference between coefficients in a row, the bispectrum at near angles outperforms the range profiles with stock aircraft.

Test Cases \ Library Aircraft	A320	EA6B	F4	F14	F15	F16	FA18	MiG	Su27	UH60
A320	0.5859	0.6245	0.5563	0.5227	0.5063	0.5626	0.5873	0.5472	0.4623	0.5948
EA6B	0.5374	0.6372	0.5438	0.5398	0.5104	0.5860	0.5207	0.5268	0.5134	0.5597
F4	0.4987	0.5290	0.6213	0.5182	0.5292	0.5310	0.5459	0.5345	0.4829	0.5593
F14	0.5034	0.4992	0.5084	0.5875	0.4992	0.4987	0.5073	0.4869	0.4657	0.5030
F15	0.5037	0.5252	0.5432	0.5131	0.6408	0.5395	0.5756	0.5721	0.5742	0.5502
F16	0.5573	0.5420	0.5248	0.5700	0.5204	0.6393	0.5503	0.5279	0.5176	0.5834
FA18	0.5121	0.5121	0.5550	0.5039	0.5272	0.5535	0.6068	0.5992	0.5042	0.5425
MiG29	0.4841	0.4986	0.5628	0.5327	0.5254	0.5376	0.5552	0.5997	0.4821	0.5349
Su27	0.4796	0.4809	0.4798	0.4862	0.5250	0.4983	0.5011	0.4769	0.5603	0.4884
UH60	0.5823	0.5757	0.6320	0.5890	0.6250	0.6516	0.5988	0.6221	0.5221	0.7249

Table 7. HBW Bispectrum Simulation With Stock Aircraft at Far Angles

Test Cases \ Library Aircraft	A320	EA6B	F4	F14	F15	F16	FA18	MiG	Su27	UH60
A320	0.6370	0.5752	0.5620	0.5332	0.5612	0.5354	0.5272	0.5517	0.5109	0.5664
EA6B	0.4747	0.6862	0.5164	0.4709	0.5441	0.5177	0.4977	0.5004	0.5095	0.4749
F4	0.5084	0.4841	0.6437	0.4974	0.4999	0.5045	0.5304	0.5467	0.5015	0.5207
F14	0.4753	0.4601	0.4733	0.6377	0.5118	0.5100	0.5237	0.4691	0.5025	0.4520
F15	0.4706	0.5224	0.4788	0.5102	0.5832	0.4863	0.4788	0.4990	0.4675	0.4512
F16	0.5446	0.5749	0.5841	0.5334	0.5680	0.6866	0.5885	0.5551	0.5268	0.5964
FA18	0.4955	0.5256	0.5368	0.5173	0.5375	0.5717	0.5956	0.5601	0.5132	0.5227
MiG29	0.4591	0.4946	0.5395	0.5453	0.5305	0.5404	0.5226	0.6178	0.5060	0.4910
Su27	0.4248	0.4426	0.4269	0.4894	0.4996	0.4593	0.4920	0.4667	0.5772	0.4110
UH60	0.6245	0.5797	0.6513	0.5536	0.5427	0.6139	0.5947	0.6255	0.5536	0.7486

Table 8. HBW Bispectrum Simulation With Stock Aircraft at Near Angles

Now let's look at how the two methods performed with the armed aircraft test sets. The first test set includes armed aircraft at angles included in the library and the second set used the same angles as the second stock set. Tables 9 and 10 show the results. The first row includes zeroes because there were no A320 test cases. The range profile simulation with the first set produced an individual success rate of 73%. After averaging, the simulation chose the correct identification every time with the first set with high correlation coefficients. The EA-6B, MiG-29, and Su-27 had the highest coefficients of the set as those aircraft were armed with only a couple extra missiles. The other aircraft were changed more with the addition of a variety of ordinance and external fuel tanks, and their coefficients were reduced as a result. The second set produced an individual success rate of only 27% and after averaging, only 4 of the aircraft were correctly identified. These aspects had less than 1^{o} of deviation from the library but the extra change provided by the configurations caused more stress on the simulation.

Test Cases \ Library Aircraft	A320	EA6B	F4	F14	F15	F16	FA18	MiG	Su27	UH60
A320	0.0000	0.0000	0.0000	0.0000	0.0000	0.0000	0.0000	0.0000	0.0000	0.0000
EA6B	0.8229	0.9706	0.8465	0.8329	0.8353	0.8266	0.8450	0.8448	0.8412	0.8456
F4	0.7517	0.7822	0.8653	0.8051	0.8312	0.8160	0.8234	0.8164	0.7984	0.7931
F14	0.7517	0.7728	0.8172	0.8629	0.8316	0.8199	0.8072	0.8157	0.8101	0.7850
F15	0.7721	0.7729	0.8080	0.7821	0.8850	0.7764	0.8031	0.8108	0.7795	0.7559
F16	0.8164	0.8365	0.8611	0.8472	0.8591	0.9374	0.8599	0.8514	0.8383	0.8485
FA18	0.8085	0.8104	0.8304	0.8246	0.8231	0.8395	0.8747	0.8017	0.8110	0.8413
MiG29	0.7672	0.8145	0.8148	0.8112	0.8221	0.8293	0.8318	0.9628	0.8143	0.8054
Su27	0.7804	0.8026	0.8167	0.8117	0.8012	0.8036	0.8139	0.8116	0.9405	0.7903
UH60	0.8252	0.8102	0.8715	0.8303	0.8409	0.8652	0.8506	0.8359	0.8306	0.8797

Table 9. HBW Range Profile Simulation With Armed Aircraft at Exact Angles

Test Cases \ Library Aircraft	A320	EA6B	F4	F14	F15	F16	FA18	MiG	Su27	UH60
A320	0.0000	0.0000	0.0000	0.0000	0.0000	0.0000	0.0000	0.0000	0.0000	0.0000
EA6B	0.7445	0.8420	0.7743	0.7683	0.7840	0.7724	0.7722	0.7975	0.7987	0.7548
F4	0.7505	0.8090	0.8177	0.8250	0.8248	0.8298	0.8123	0.8329	0.7917	0.7951
F14	0.7828	0.8177	0.8162	0.8148	0.8096	0.8095	0.8049	0.8108	0.8007	0.8149
F15	0.7940	0.8032	0.8275	0.8205	0.8102	0.8225	0.8311	0.8251	0.8208	0.8064
F16	0.7596	0.8052	0.7933	0.8149	0.7956	0.8154	0.8071	0.8034	0.7835	0.7697
FA18	0.7968	0.8271	0.8427	0.8278	0.8299	0.8413	0.8507	0.8330	0.8228	0.8456
MiG29	0.7513	0.8003	0.8411	0.8178	0.8070	0.8212	0.8171	0.8401	0.8087	0.7838
Su27	0.7282	0.7664	0.7654	0.7556	0.7490	0.7375	0.7471	0.7435	0.8064	0.7409
UH60	0.8423	0.8491	0.8905	0.8587	0.8767	0.8809	0.8993	0.8631	0.8466	0.8989

Table 10. HBW Range Profile Simulation With Armed Aircraft at Near Angles

The bispectrum simulation was able to handle these two test sets more easily. The first set produced an individual success rate of 80%. After averaging, the simulation correctly identified every aircraft as did the range profile simulation. The effect of the varying levels of configuration change is more easily noticed with the coefficients produced by the bispectrum. The slightly changed aircraft maintained coefficients around 0.9 contrasting with the most heavily armed F/A-18 with a coefficient of only 0.57. The second test set was again harder to manage for the simulation. It produced an individual success rate of 49%, but much greater than the 27% for the range profile based target identification. After averaging though, 7 of the 9 aircraft were correctly identified, thus outperforming the range profile's 4 identifications. In the two test rows that were misidentified, the correct aircraft came in second place by a small margin. Tables 11 and 12 contain the results.

Test Cases \ Library Aircraft	A320	EA6B	F4	F14	F15	F16	FA18	MiG	Su27	UH60
A320	0.0000	0.0000	0.0000	0.0000	0.0000	0.0000	0.0000	0.0000	0.0000	0.0000
EA6B	0.5546	0.9218	0.5800	0.5879	0.5878	0.6036	0.5794	0.5993	0.5282	0.6217
F4	0.4795	0.4549	0.7063	0.5024	0.5219	0.5285	0.5088	0.5309	0.5405	0.5346
F14	0.4609	0.5031	0.5207	0.6136	0.5128	0.5406	0.5175	0.5181	0.4767	0.4876
F15	0.5533	0.5442	0.5694	0.5391	0.7889	0.5782	0.5804	0.5860	0.4954	0.5482
F16	0.5916	0.6325	0.6038	0.6089	0.5774	0.8432	0.6356	0.5969	0.5350	0.6400
FA18	0.4892	0.5158	0.5366	0.5297	0.5223	0.5573	0.5698	0.5113	0.5181	0.5306
MiG29	0.4652	0.5026	0.5353	0.4902	0.5254	0.5133	0.5009	0.9064	0.4971	0.4995
Su27	0.4221	0.4443	0.4519	0.4435	0.4859	0.4326	0.4523	0.4707	0.8632	0.4174
UH60	0.5851	0.5758	0.6170	0.5961	0.5701	0.6467	0.6185	0.5630	0.5612	0.6554

Table 11. HBW Bispectrum Simulation With Armed Aircraft at Exact Angles

Test Cases \ Library Aircraft	A320	EA6B	F4	F14	F15	F16	FA18	MiG	Su27	UH60
A320	0.0000	0.0000	0.0000	0.0000	0.0000	0.0000	0.0000	0.0000	0.0000	0.0000
EA6B	0.4712	0.6638	0.5023	0.4633	0.5430	0.5128	0.4887	0.5024	0.5011	0.4819
F4	0.4612	0.4799	0.5474	0.4850	0.4903	0.5295	0.5177	0.5444	0.4844	0.4980
F14	0.4731	0.4777	0.4833	0.5837	0.5237	0.4872	0.5139	0.4837	0.4809	0.4755
F15	0.4785	0.5339	0.4662	0.5458	0.5425	0.5315	0.5147	0.4746	0.5358	0.4693
F16	0.4829	0.5359	0.5139	0.5070	0.5233	0.6025	0.5398	0.5280	0.5077	0.5168
FA18	0.5101	0.5117	0.5796	0.5030	0.5509	0.5313	0.5694	0.5510	0.4903	0.5446
MiG29	0.4482	0.4834	0.5133	0.5133	0.5052	0.4924	0.5151	0.5786	0.4777	0.4821
Su27	0.4650	0.4574	0.4583	0.4693	0.4871	0.4789	0.4796	0.4814	0.5035	0.4534
UH60	0.5482	0.5777	0.6048	0.5058	0.5685	0.5882	0.6383	0.5876	0.5243	0.6551

Table 12. HBW Bispectrum Simulation With Armed Aircraft at Near Angles

2. Low Bandwidth Results

The reduction in the ability to distinguish structures on the aircraft caused the low bandwidth (LBW) simulations to produce worse results. The range profile simulations with the stock aircraft configurations produced an individual success rate of 40% for the far angles and 48% for the near angles. Both these are lower than the 60% for the HBW cases. After averaging, the simulation failed to correctly identify the F-15 for the far angles. Curiously, with the near angles, it failed with the F-14, F-16, and MiG-29. The difference must lie in the particular angles chosen for the different test sets. Since the LBW cases are not as rotationally variant, there should be less difference between the near and far angle cases. Despite having a better individual success rate, the second set underperformed the first set after averaging. The troublesome issue with these simulations was the very narrow margin between the correct and incorrect identifications. Tables 13 and 14 show the results.

Test Cases \ Library Aircraft	A320	EA6B	F4	F14	F15	F16	FA18	MiG	Su27	UH60
A320	0.8719	0.8201	0.8172	0.8095	0.8332	0.8091	0.8001	0.7931	0.8205	0.8062
EA6B	0.8369	0.9041	0.8330	0.8554	0.8558	0.8620	0.8476	0.8484	0.8487	0.8325
F4	0.8603	0.8909	0.9208	0.9032	0.9152	0.9045	0.9045	0.9050	0.8852	0.8897
F14	0.8544	0.8879	0.8848	0.9132	0.8886	0.9094	0.9077	0.8784	0.8866	0.8598
F15	0.8726	0.8901	0.9157	0.8897	0.9162	0.9053	0.9071	0.9263	0.9020	0.8921
F16	0.8991	0.8928	0.9192	0.9193	0.9211	0.9318	0.9168	0.9092	0.9010	0.9228
FA18	0.8746	0.8858	0.9156	0.9027	0.9123	0.9161	0.9225	0.9174	0.9167	0.9017
MiG29	0.8580	0.8868	0.8977	0.8831	0.8967	0.9117	0.9036	0.9250	0.8790	0.8933
Su27	0.8764	0.9141	0.8974	0.9108	0.9071	0.9056	0.9017	0.9025	0.9196	0.8873
UH60	0.9119	0.8963	0.9292	0.9086	0.9233	0.9307	0.9069	0.9006	0.8813	0.9426

Table 13. LBW Range Profile Simulation With Stock Aircraft at Far Angles

Test Cases \ Library Aircraft	A320	EA6B	F4	F14	F15	F16	FA18	MiG	Su27	UH60
A320	0.8966	0.8376	0.8152	0.8403	0.8335	0.8338	0.8040	0.8108	0.8233	0.8248
EA6B	0.8541	0.9284	0.8665	0.8685	0.8918	0.8634	0.8734	0.8765	0.8858	0.8515
F4	0.8676	0.8811	0.9287	0.8899	0.9064	0.8980	0.8915	0.9063	0.8807	0.8758
F14	0.8309	0.8670	0.8659	0.8934	0.8856	0.8944	0.8718	0.8619	0.8764	0.8618
F15	0.8476	0.8835	0.8914	0.9031	0.9107	0.9021	0.8885	0.8906	0.8947	0.8544
F16	0.8691	0.9027	0.9148	0.9027	0.9209	0.9208	0.9143	0.8982	0.9111	0.9037
FA18	0.8957	0.8947	0.9333	0.9113	0.9116	0.9167	0.9380	0.9263	0.9109	0.9257
MiG29	0.9073	0.8861	0.9246	0.9143	0.9161	0.9142	0.9274	0.9259	0.9128	0.9119
Su27	0.8443	0.8775	0.8784	0.8729	0.8802	0.8621	0.8762	0.8885	0.9030	0.8631
UH60	0.9120	0.9226	0.9406	0.9267	0.9302	0.9398	0.9405	0.9097	0.9228	0.9539

Table 14. LBW Range Profile Simulation With Stock Aircraft at Near Angles

The bispectrum simulation with the first test set produced an individual success rate of 56% outperforming the range profile, but still failed to identify the F-15 after averaging. The success rate is on par with the 58% achieved with the HBW set. The second test set with near angles produced an individual success rate of 42% while misidentifying two aircraft after averaging. As with the range profile simulation, the bispectrum simulation was not as effective with near angles as with far angles at LBW. The LBW did produce greater correlation coefficients than with the same test cases at HBW. Tables 15 and 16 show the results. As expected though, the HBW stock cases for both the bispectrum and the range profile outperformed the LBW simulations.

Test Cases \ Library Aircraft	A320	EA6B	F4	F14	F15	F16	FA18	MiG	Su27	UH60
A320	0.7032	0.5854	0.5736	0.5545	0.5445	0.5837	0.5574	0.5710	0.5479	0.6033
EA6B	0.5793	0.7222	0.5959	0.5939	0.6009	0.5838	0.6040	0.6058	0.6018	0.5412
F4	0.6396	0.6468	0.7387	0.6802	0.6912	0.7266	0.6952	0.6814	0.6709	0.6686
F14	0.5866	0.6369	0.6614	0.6984	0.6404	0.6879	0.6733	0.6484	0.6477	0.5977
F15	0.6444	0.7063	0.7158	0.7084	0.7151	0.7136	0.7143	0.7370	0.7020	0.6594
F16	0.6582	0.6911	0.7039	0.7089	0.7097	0.7817	0.7115	0.6932	0.6626	0.6531
FA18	0.6460	0.6621	0.6853	0.7027	0.6799	0.7002	0.7494	0.6947	0.6858	0.6479
MiG29	0.6742	0.7123	0.7428	0.6754	0.6994	0.7289	0.7176	0.7552	0.6889	0.6822
Su27	0.6512	0.6477	0.6523	0.6858	0.6625	0.6376	0.6437	0.6892	0.7518	0.5898
UH60	0.6774	0.6831	0.7328	0.6480	0.6730	0.7386	0.7422	0.7151	0.6665	0.7602

Table 15. LBW Bispectrum Simulation With Stock Aircraft at Far Angles

Test Cases \ Library Aircraft	A320	EA6B	F4	F14	F15	F16	FA18	MiG	Su27	UH60
A320	0.7265	0.5947	0.5073	0.5889	0.5516	0.5719	0.5634	0.5928	0.5904	0.5662
EA6B	0.6063	0.8004	0.5970	0.6362	0.6120	0.6279	0.6243	0.6444	0.6569	0.5851
F4	0.6029	0.6186	0.7462	0.6544	0.6545	0.6794	0.6414	0.6447	0.6352	0.6411
F14	0.5878	0.6164	0.6421	0.6839	0.6473	0.6546	0.6234	0.6520	0.6344	0.5771
F15	0.5704	0.6048	0.6620	0.6661	0.6950	0.6705	0.6474	0.6555	0.6574	0.5599
F16	0.6330	0.6170	0.6372	0.6545	0.6438	0.6937	0.6845	0.6600	0.6493	0.6046
FA18	0.6608	0.7057	0.7347	0.6880	0.7143	0.7354	0.7319	0.7271	0.6878	0.7153
MiG29	0.7007	0.7133	0.7274	0.6965	0.7254	0.7521	0.7328	0.7490	0.7136	0.6950
Su27	0.5605	0.6162	0.6202	0.6338	0.6369	0.6450	0.6310	0.6350	0.7318	0.5676
UH60	0.7398	0.7396	0.7769	0.7064	0.7181	0.7940	0.7582	0.7619	0.7422	0.8148

Table 16. LBW Bispectrum Simulation With Stock Aircraft at Near Angles

The hypothesis was that configuration changes would have less effect with LBW cases because of the reduced ability to pick out the changes in the profiles. This generally held true. The range profile simulation with the first test set of armed aircraft produced an individual success rate of 71% and misidentified one aircraft after averaging. Correlation coefficients were all higher compared to the same test set at HBW. The second test set produced a success rate of 36% and misidentified 3 of the 9 aircraft. This 36% was only slightly worse than the second stock set with the same angles. The drastic difference of the same two test sets at HBW shows that configuration changes have less effect at LBW. Whereas the HBW range profiles outperformed the LBW sets with stock configurations, the second LBW armed set outperformed the same HBW set. Tables 17 and 18 show the results.

Test Cases \ Library Aircraft	A320	EA6B	F4	F14	F15	F16	FA18	MiG	Su27	UH60
A320	0.0000	0.0000	0.0000	0.0000	0.0000	0.0000	0.0000	0.0000	0.0000	0.0000
EA6B	0.7925	0.9830	0.8700	0.8457	0.8747	0.8464	0.8434	0.8772	0.8739	0.8282
F4	0.8805	0.8778	0.9093	0.9009	0.8993	0.9091	0.8939	0.9034	0.8875	0.8813
F14	0.8375	0.8631	0.8975	0.9214	0.8769	0.8785	0.8811	0.8621	0.8710	0.8736
F15	0.8197	0.8572	0.8856	0.8886	0.9134	0.8825	0.8751	0.8848	0.8628	0.8747
F16	0.8559	0.8986	0.9084	0.8914	0.8992	0.9460	0.9054	0.9091	0.8880	0.9012
FA18	0.8816	0.9020	0.9180	0.9176	0.9093	0.9067	0.9177	0.9177	0.9128	0.9018
MiG29	0.8475	0.8879	0.9061	0.9078	0.9016	0.8959	0.8981	0.9629	0.8911	0.8888
Su27	0.8663	0.9037	0.9012	0.8916	0.8863	0.8878	0.8986	0.9017	0.9698	0.8859
UH60	0.9175	0.8982	0.9247	0.9111	0.9040	0.9298	0.9276	0.9183	0.8975	0.9390

Table 17. LBW Range Profile Simulation With Armed Aircraft at Exact Angles

Test Cases \ Library Aircraft	A320	EA6B	F4	F14	F15	F16	FA18	MiG	Su27	UH60
A320	0.0000	0.0000	0.0000	0.0000	0.0000	0.0000	0.0000	0.0000	0.0000	0.0000
EA6B	0.8407	0.9239	0.8688	0.8700	0.8885	0.8628	0.8583	0.8798	0.8772	0.8416
F4	0.8317	0.8689	0.8868	0.8667	0.8932	0.8855	0.8615	0.8831	0.8870	0.8643
F14	0.8240	0.8512	0.8589	0.9009	0.8743	0.8847	0.8640	0.8586	0.8642	0.8490
F15	0.8484	0.8878	0.8821	0.8874	0.9065	0.8766	0.8780	0.8860	0.8797	0.8652
F16	0.8589	0.8904	0.9108	0.9087	0.9111	0.9110	0.9104	0.8952	0.9022	0.8872
FA18	0.8629	0.8757	0.8919	0.8973	0.9025	0.8992	0.9038	0.9034	0.8957	0.8845
MiG29	0.9127	0.8900	0.9236	0.9228	0.9119	0.9278	0.9310	0.9223	0.9154	0.9184
Su27	0.8058	0.8403	0.8496	0.8559	0.8545	0.8286	0.8386	0.8452	0.8648	0.8358
UH60	0.9126	0.9008	0.9233	0.9066	0.9145	0.9311	0.9205	0.9105	0.9152	0.9393

Table 18. LBW Range Profile Simulation With Armed Aircraft at Near Angles

The bispectrum simulations with armed aircraft followed closely with the same range profile simulations. The first test set had a success rate of 73% and misidentified one aircraft after averaging. This bispectrum set produced a bigger difference between the coefficients for the correct and incorrect aircraft than the same range profile set. This creates a stronger likely identification. The second test set had a success rate of 40% and misidentified 2 aircraft slightly outperforming the same range profile set. This second armed test set closely matches the performance of the second stock test set again showing that the LBW simulations are less affected by configuration changes. The LBW bispectrum armed test sets only perform slightly worse than the same sets at HBW. Tables 19 and 20 show the results.

Test Cases \ Library Aircraft	A320	EA6B	F4	F14	F15	F16	FA18	MiG	Su27	UH60
A320	0.0000	0.0000	0.0000	0.0000	0.0000	0.0000	0.0000	0.0000	0.0000	0.0000
EA6B	0.5266	0.9492	0.6065	0.6111	0.6179	0.5896	0.6182	0.6237	0.6087	0.5564
F4	0.6144	0.6438	0.7507	0.6653	0.6885	0.7224	0.6794	0.6651	0.6857	0.6582
F14	0.6193	0.6281	0.6913	0.7903	0.6637	0.6929	0.6659	0.6856	0.6358	0.6523
F15	0.5443	0.6041	0.6198	0.6664	0.7988	0.6336	0.6618	0.6464	0.6239	0.5919
F16	0.6935	0.7153	0.7139	0.7261	0.7155	0.8858	0.7116	0.7503	0.6765	0.7526
FA18	0.6631	0.6855	0.7142	0.7218	0.7356	0.7091	0.7308	0.6725	0.6692	0.6474
MiG29	0.6124	0.6746	0.6764	0.6598	0.6920	0.6617	0.6723	0.8859	0.6717	0.6552
Su27	0.6457	0.6638	0.6318	0.6573	0.6585	0.6362	0.6563	0.6478	0.9113	0.5406
UH60	0.7248	0.7405	0.7916	0.7059	0.7013	0.8072	0.7794	0.7642	0.6878	0.8175

Table 19. LBW Bispectrum Simulation With Armed Aircraft at Exact Angles

Test Cases \ Library Aircraft	A320	EA6B	F4	F14	F15	F16	FA18	MiG	Su27	UH60
A320	0.0000	0.0000	0.0000	0.0000	0.0000	0.0000	0.0000	0.0000	0.0000	0.0000
EA6B	0.6209	0.7611	0.5922	0.6549	0.6215	0.6129	0.6123	0.6463	0.6427	0.5706
F4	0.5543	0.6289	0.6424	0.6038	0.6418	0.6531	0.6283	0.6346	0.6001	0.5711
F14	0.5541	0.6290	0.6533	0.6764	0.6458	0.6351	0.6444	0.6404	0.6008	0.5633
F15	0.5674	0.6135	0.6661	0.6449	0.6806	0.6240	0.6577	0.6496	0.6543	0.5851
F16	0.5878	0.6204	0.6492	0.6465	0.6427	0.6995	0.6580	0.6387	0.6270	0.6020
FA18	0.6141	0.6434	0.7111	0.6749	0.6638	0.7158	0.7187	0.7063	0.6704	0.6493
MiG29	0.6945	0.7070	0.7179	0.6805	0.7149	0.7353	0.7391	0.7205	0.7220	0.6994
Su27	0.5498	0.5839	0.5650	0.5954	0.5864	0.5729	0.5791	0.5951	0.6756	0.5031
UH60	0.6833	0.7470	0.7807	0.7244	0.6958	0.7610	0.7639	0.7089	0.7069	0.7958

Table 20. LBW Bispectrum Simulation With Armed Aircraft at Near Angles

THIS PAGE INTENTIONALLY LEFT BLANK

VII. CONCLUSIONS

A. SUMMARY

Military members make life or death decisions based on the set of information they have at their disposal at the instant the decision needs to be made. A basic component of that information is the question of whether the contact about to be destroyed is an enemy or a friend. Any hesitation made by the operator as a result of not trusting the identification being presented by his system can be fatal. The goal is to maximize the quality of the information he receives in order to build the trust that when the system tells the operator the contact is an incoming F-16, he knows that it is. In instances where this information was not present, or where it was incorrect, the resulting consequences were shown.

A radar system detects contacts by sending and receiving electromagnetic energy and processing the received signal. The basic hardware layout was described and how radar parameters such as beam width, pulse width, bandwidth, and frequency affect the ability of the system to resolve targets. The electromagnetic energy interacts with the target and scatters to form unique signatures. The RCS codes used in the simulation estimate the scattered field by summing contributions from physical optics, the physical theory of diffraction, and multiple interactions. By analyzing the scattered field we can try to determine what kind of contact created the field. A library of various aircraft was created to facilitate the comparison of the range profile and bispectrum methods of identification.

B. EFFECTIVENESS

It was shown through a series of simulations that a system using bispectrum correlation meets or exceeds the performance of a system using range profile correlation. The bispectrum produced a 5.3% increase in identification accuracy over range profiles after averaging in both the HBW and LBW simulations. The results are summarized in Tables 21 and 22. Future sensor systems should have an increased bandwidth over current systems which make techniques such as the bispectrum more promising.

	Range Prof	Bispectrum
Individual	55.0 %	66.8 %
Averaged	86.8 %	92.1 %

Table 21. Results Summary for High Bandwidth Simulation

	Range Prof	Bispectrum
Individual	48.8 %	52.8 %
Averaged	78.9 %	84.2 %

Table 22. Results Summary for Low Bandwidth Simulation

The various success rates shown throughout the thesis are not impressive, but they should not be considered as stand-alone figures. The library used to search through was very coarse and is only useful to have a standard to compare the two algorithms side-by-side. Also, much more advanced signal processing techniques can be used to refine the methods. Standard methods, initial conditions, and test cases were employed in the simulation, allowing direct comparison between the methods.

No one method should be used for identification; rather, many methods can be combined in a hybrid system. For instance, since the range profile system takes significantly less time to run, the field of possible matches can be quickly narrowed using range profiles, and then the likely matches can be further analyzed with the bispectrum. Also, weighting factors can be applied based on the likelihood of that contact actually being present in a certain region. Many clever techniques have been developed for identification, but this thesis shows that using the bispectrum should remain a part of that set.

C. ADDITIONAL CONSIDERATIONS

More factors go into the determination of a good identification method than were considered in this simulation. Implementation issues such as speed of execution, efficiency of the algorithms, and size of storage required to hold the library should be also considered. For instance, the bispectrum simulation used in the thesis took over six minutes per test case to search through the entire library on a modern computer. The range profile simulation took just over six seconds per test case. Additionally, the library

of range profiles took up only a couple of megabytes of storage space whereas the library of bispectra took up three orders of magnitude greater than that. Correlating with a data set that would have to be much larger than this is not a trivial process.

The effect of noise was also not considered. The very faint radar returns of distant targets are full of noise and can drastically affect the identification ability. It has been shown that the bispectrum suppresses additive Gaussian noise, which may give it an additional advantage over the range profiles [24]-[28]. The addition of different levels of noise into the test cases should be considered to determine the signal-to-noise ratio when these methods break down.

The polarizations used for the returns in this thesis were the horizontally transmitted, horizontally received polarizations. Vertical or cross polarizations should be considered to see if the bispectrum is more useful with multiple polarization information. It may be that multiple interaction scattering tends to produces certain polarizations and that could be exploited with the bispectrum.

Clutter was added into the simulation in the form of configuration changes. A real library might have multiple standard configurations of aircraft already considered so additional clutter should also be added. Whether this method would be useful in clutter filled areas such as against vehicles on the ground or ships on choppy waters should be determined. The current styles of ships in the fleets of the world have so many external structures to facilitate multiple interactions that the bispectrum would likely be a useful tool to identify distant ships.

THIS PAGE INTENTIONALLY LEFT BLANK

APPENDIX

A. AIRCRAFT USED IN SIMULATION

Figure 26. Airbus A320

Figure 27. EA-6B Prowler

Figure 28. F-4N Phantom II

Figure 29. F-14D Tomcat

Figure 30. F-15E Strike Eagle

Figure 31. F-16C Falcon

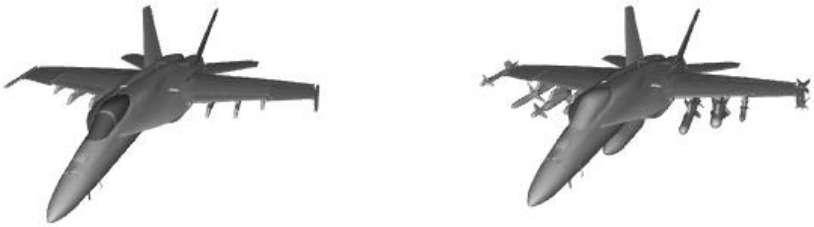

Figure 32. F/A-18E Super Hornet

Figure 33. MiG-29A Fulcrum

Figure 34. Su-27 Flanker B

Figure 35. UH-60L Black Hawk

B. LIST OF TEST CASES

		Stock		Stock2				Dirty		Dirty2	
Case	Aircraft	θ	Φ	θ	Φ	Case	Aircraft	θ	Φ	θ	Φ
01	a320	072	002	100	000.5	01	ea6b	090	000	100	000.5
02	a320	112	007	081	009	02	ea6b	105	015	081	009
03	a320	097	023	086	024.5	03	ea6b	075	024	086	024.5
04	a320	078	035	100	031	04	ea6b	085	033	100	031
05	a320	108	037	091	040	05	ea6b	120	045	091	040
06	ea6b	072	002	100	000.5	06	f4	090	000	100	000.5
07	ea6b	112	007	081	009	07	f4	105	015	081	009
08	ea6b	097	023	086	024.5	08	f4	075	024	086	024.5
09	ea6b	078	035	100	031	09	f4	085	033	100	031
10	ea6b	108	037	091	040	10	f4	120	045	091	040
11	f4	072	002	100	000.5	11	f14	090	000	100	000.5
12	f4	112	007	081	009	12	f14	105	015	081	009
13	f4	097	023	086	024.5	13	f14	075	024	086	024.5
14	f4	078	035	100	031	14	f14	085	033	100	031
15	f4	108	037	091	040	15	f14	120	045	091	040
16	f14	072	002	100	000.5	16	f15	090	000	100	000.5
17	f14	112	007	081	009	17	f15	105	015	081	009
18	f14	097	023	086	024.5	18	f15	075	024	086	024.5
19	f14	078	035	100	031	19	f15	085	033	100	031
20	f14	108	037	091	040	20	f15	120	045	091	040
21	f15	072	002	100	000.5	21	f16	090	000	100	000.5
22	f15	112	007	081	009	22	f16	105	015	081	009
23	f15	097	023	086	024.5	23	f16	075	024	086	024.5
24	f15	078	035	100	031	24	f16	085	033	100	031
25	f15	108	037	091	040	25	f16	120	045	091	040
26	f16	072	002	100	000.5	26	fa18	090	000	100	000.5
27	f16	112	007	081	009	27	fa18	105	015	081	009
28	f16	097	023	086	024.5	28	fa18	075	024	086	024.5
29	f16	078	035	100	031	29	fa18	085	033	100	031
30	f16	108	037	091	040	30	fa18	120	045	091	040
31	fa18	072	002	100	000.5	31	mig29	090	000	100	000.5
32	fa18	112	007	081	009	32	mig29	105	015	081	009
33	fa18	097	023	086	024.5	33	mig29	075	024	086	024.5
34	fa18	078	035	100	031	34	mig29	085	033	100	031
35	fa18	108	037	091	040	35	mig29	120	045	091	040
36	mig29	072	002	100	000.5	36	su27	090	000	100	000.5
37	mig29	112	007	081	009	37	su27	105	015	081	009
38	mig29	097	023	086	024.5	38	su27	075	024	086	024.5
39	mig29	078	035	100	031	39	su27	085	033	100	031
40	mig29	108	037	091	040	40	su27	120	045	091	040
41	su27	072	002	100	000.5	41	uh60	090	000	100	000.5
42	su27	112	007	081	009	42	uh60	105	015	081	009
43	su27	097	023	086	024.5	43	uh60	075	024	086	024.5
44	su27	078	035	100	031	44	uh60	085	033	100	031
45	su27	108	037	091	040	45	uh60	120	045	091	040
46	uh60	072	002	100	000.5						
47	uh60	112	007	081	009						
48	uh60	097	023	086	024.5						
49	uh60	078	035	100	031						
50	uh60	108	037	091	040						

C. BISPECTRUM CODE

```
% **********************  getBi.m   **********************
% LT Zachary Cole, USN
% Naval Postgraduate School - Physics

% This function calculates and returns the bispectrum of the input signal.
% function adapted from code by Jiunn Wah Yeo [11]

% signal is the freq domain complex scattered field

function output = getBi(signal);

% ------------------------------------------------------------
% generate third order cumulant of signal

signal_length = length(signal)-1;

% Assignment and pre-conditioning of signal
signal_conj=conj(signal(:));
signal_col=signal(:);

N = length(signal_conj);

% Triple correlation of signal
X1 = repmat(signal_conj,1,2*signal_length+1);

C2=[zeros(signal_length,1);signal_col(1:signal_length+1)];
R2=[signal_col(signal_length+1:N).' zeros(1,signal_length)];
X2=hankel(C2,R2);
X3=X2.';

cum3=X2*(X1.*X3)/N;   % 3rd order cumulant

% ------------------------------------------------------------
% Perform Fourier Transform of the third order cumulant to
% generate the bispectrum

output = fftshift(fft2(ifftshift(cum3)));   % bispectrum
```

D. SIMULATION CODE

```
% **********************   p_corr_sim.m    **********************
% LT Zachary Cole, USN
% Naval Postgraduate School - Physics

% RUN TIME: 5 minutes

% This file implements a cross correlation classification scheme
% for range profiles.

% This is the general program control flow for running the correlation
% simulation.  It is broken up into 4 main loops.  Each loop cycles through
% the a set of test cases based on 10 aircraft for stock configurations
% and 9 aircraft for armed configurations according to the table below.  It
% creates 6 output files, one for each loop and 2 for consolidating the
% different bin matrices.

% inputs:
% p_stock   same configs as library at angles far from library (1-3 deg)
% p_stock2  same configs as library at angles closer to library (<=1 deg)
% p_dirty   armed aircraft at angles corresponding to library (0 deg)
% p_dirty2  armed aircraft at same angles as stock2
```

```
% lookup_table  a text array for displaying user friendly results
% ../zLibrary/  holds the library of aircraft

% class_array -- an array of 2080 correlation coefficients from comparing
% one test case to the library.
% index -- the maximum corr coef in the array

% helper files: checkLibraryCORRP.m, rowS.m, rowD.m, column.m,
% fillRowWithCoefs.m, howCorrP.m, ../zLibrary/

clear;

load lookup_table;

% these are the matrices for individual identifications
bin_matrix_s = zeros(10,10);
bin_matrix_s2 = zeros(10,10);
bin_matrix_d = zeros(10,10);
bin_matrix_d2 = zeros(10,10);

% these are the matrices for averaged correlation coefficients
coef_matrix_s = zeros(10,10);
coef_matrix_s2 = zeros(10,10);
coef_matrix_d = zeros(10,10);
coef_matrix_d2 = zeros(10,10);

out = fopen('p_corr_stock_results.txt','wt'); %open file for results
fprintf(out, 'p_stock corr tests\n');
load p_stock;  %load test case set
for testcase = 1:50
   % check one test case with library
   class_array = checkLibraryCORRP(p_stock{testcase});
   % find most likely aircraft
   index=find(class_array==max(class_array));
   % fill matrix with coefficients
   coef_matrix_s(rowS(testcase),:) = coef_matrix_s(rowS(testcase),:) + fillRowWithCoefs(class_array);
   % fill binary matrix with likely identification
   bin_matrix_s(rowS(testcase),column(index))=bin_matrix_s(rowS(testcase),column(index))+1;
   fprintf(out, '%3g   %s\n',testcase, lookup_table(index,:));
end
clear p_stock;
coef_matrix_s = coef_matrix_s / 5; %average matrix (5 cases per aircraft)
fclose(out);

out = fopen('p_corr_stock2_results.txt','wt'); %open file for results
fprintf(out, 'p_stock2 corr tests\n');
load p_stock2;  %load test case set
for testcase = 1:50
   % check one test case with library
   class_array = checkLibraryCORRP(p_stock2{testcase});
   % find most likely aircraft
   index=find(class_array==max(class_array));
   % fill matrix with coefficients
   coef_matrix_s2(rowS(testcase),:) = coef_matrix_s2(rowS(testcase),:) + fillRowWithCoefs(class_array);
   % fill binary matrix with likely identification
   bin_matrix_s2(rowS(testcase),column(index))=bin_matrix_s2(rowS(testcase),column(index))+1;
   fprintf(out, '%3g   %s\n',testcase, lookup_table(index,:));
end
clear p_stock2;
coef_matrix_s2 = coef_matrix_s2 / 5; %average matrix (5 cases per aircraft)
fclose(out);

out = fopen('p_corr_dirty_results.txt','wt'); %open file for results
fprintf(out, 'p_dirty corr tests\n');
load p_dirty;  %load test case set
for testcase = 1:45
   % check one test case with library
   class_array = checkLibraryCORRP(p_dirty{testcase});
```

```
   % find most likely aircraft
   index=find(class_array==max(class_array));
   % fill matrix with coefficients
   coef_matrix_d(rowD(testcase),:) = coef_matrix_d(rowD(testcase),:) + fillRowWithCoefs(class_array);
   % fill binary matrix with likely identification
   bin_matrix_d(rowD(testcase),column(index))=bin_matrix_d(rowD(testcase),column(index))+1;
   fprintf(out, '%3g   %s\n',testcase, lookup_table(index,:));
end
clear p_dirty;
coef_matrix_d = coef_matrix_d / 5; %average matrix (5 cases per aircraft)
fclose(out);

out = fopen('p_corr_dirty2_results.txt','wt'); %open file for results
fprintf(out, 'p_dirty2 corr tests\n');
load p_dirty2;  %load test case set
for testcase = 1:45
   % check one test case with library
   class_array = checkLibraryCORRP(p_dirty2{testcase});
   % find most likely aircraft
   index=find(class_array==max(class_array));
   % fill matrix with coefficients
   coef_matrix_d2(rowD(testcase),:) = coef_matrix_d2(rowD(testcase),:) + fillRowWithCoefs(class_array);
   % fill binary matrix with likely identification
   bin_matrix_d2(rowD(testcase),column(index))=bin_matrix_d2(rowD(testcase),column(index))+1;
   fprintf(out, '%3g   %s\n',testcase, lookup_table(index,:));
end
clear p_dirty2;
coef_matrix_d2 = coef_matrix_d2 / 5; %average matrix (5 cases per aircraft)
fclose(out);

% Consolidate and print results to a file
% results will be matrices where rows correspond to test case platforms (5
% each) and columns correspond to library identifications by aircraft type.
out = fopen('p_matrix_bin.txt','wt');
fprintf(out, 'p_stock corr tests\n\n');
fprintf(out, 'A320 EA6B F4   F14  F15  F16  FA18 MiG  Su27 UH60\n');
fprintf(out, '%1.0f   %1.0f   %1.0f   %1.0f   %1.0f   %1.0f   %1.0f   %1.0f   %1.0f   %1.0f  \n', bin_matrix_s');
fprintf(out, '\np_stock2 corr tests\n\n');
fprintf(out, 'A320 EA6B F4   F14  F15  F16  FA18 MiG  Su27 UH60\n');
fprintf(out, '%1.0f   %1.0f   %1.0f   %1.0f   %1.0f   %1.0f   %1.0f   %1.0f   %1.0f   %1.0f  \n', bin_matrix_s2');
fprintf(out, '\np_dirty corr tests\n\n');
fprintf(out, 'A320 EA6B F4   F14  F15  F16  FA18 MiG  Su27 UH60\n');
fprintf(out, '%1.0f   %1.0f   %1.0f   %1.0f   %1.0f   %1.0f   %1.0f   %1.0f   %1.0f   %1.0f  \n', bin_matrix_d');
fprintf(out, '\np_dirty2 corr tests\n\n');
fprintf(out, 'A320 EA6B F4   F14  F15  F16  FA18 MiG  Su27 UH60\n');
fprintf(out, '%1.0f   %1.0f   %1.0f   %1.0f   %1.0f   %1.0f   %1.0f   %1.0f   %1.0f   %1.0f  \n', bin_matrix_d2');
fclose(out);

% Consolidate and print results to a file
out = fopen('p_matrix_coef.txt','wt');
fprintf(out, 'p_stock corr tests\n\n');
fprintf(out, 'A320   EA6B   F4    F14   F15   F16   FA18   MiG   Su27   UH60\n');
fprintf(out, '%5.4f %5.4f %5.4f %5.4f %5.4f %5.4f %5.4f %5.4f %5.4f %5.4f\n', coef_matrix_s');
fprintf(out, '\np_stock2 corr tests\n\n');
fprintf(out, 'A320   EA6B   F4    F14   F15   F16   FA18   MiG   Su27   UH60\n');
fprintf(out, '%5.4f %5.4f %5.4f %5.4f %5.4f %5.4f %5.4f %5.4f %5.4f %5.4f\n', coef_matrix_s2');
fprintf(out, '\np_dirty corr tests\n\n');
fprintf(out, 'A320   EA6B   F4    F14   F15   F16   FA18   MiG   Su27   UH60\n');
fprintf(out, '%5.4f %5.4f %5.4f %5.4f %5.4f %5.4f %5.4f %5.4f %5.4f %5.4f\n', coef_matrix_d');
fprintf(out, '\np_dirty2 corr tests\n\n');
fprintf(out, 'A320   EA6B   F4    F14   F15   F16   FA18   MiG   Su27   UH60\n');
fprintf(out, '%5.4f %5.4f %5.4f %5.4f %5.4f %5.4f %5.4f %5.4f %5.4f %5.4f\n', coef_matrix_d2');
fclose(out);


% ********************   checkLibraryCORRP.m   **********************
% LT Zachary Cole, USN
% Naval Postgraduate School - Physics
```

```
% checkLibrary is a function that provides an array where each element
% indicates how similiar the signal is to the specific library signal.
% The array element corresponds to a lookup table of all the library
% signals.

function output_array = checkLibraryCORRP(signal);

load ../zLibrary/a320_pc;  %load a320 section of library
for index=1:208  %for the a320 section of the output_array
   output_array(index) = howCorrP(signal,a320_pc{index});
end
clear a320_pc;

load ../zLibrary/ea6b_pc;  %load ea6b section of library
for index=209:416  %for the ea6b section of the output_array
   output_array(index) = howCorrP(signal,ea6b_pc{index-208});
end
clear ea6b_pc

load ../zLibrary/f4_pc;  %load f4 section of library
for index=417:624  %for the f4 section of the output_array
   output_array(index) = howCorrP(signal,f4_pc{index-416});
end
clear f4_pc

load ../zLibrary/f14_pc;  %load f14 section of library
for index=625:832  %for the f14 section of the output_array
   output_array(index) = howCorrP(signal,f14_pc{index-624});
end
clear f14_pc

load ../zLibrary/f15_pc;  %load f15 section of library
for index=833:1040  %for the f15 section of the output_array
   output_array(index) = howCorrP(signal,f15_pc{index-832});
end
clear f15_pc

load ../zLibrary/f16_pc;  %load f16 section of library
for index=1041:1248  %for the f16 section of the output_array
   output_array(index) = howCorrP(signal,f16_pc{index-1040});
end
clear f16_pc

load ../zLibrary/fa18_pc;  %load fa18 section of library
for index=1249:1456  %for the fa18 section of the output_array
   output_array(index) = howCorrP(signal,fa18_pc{index-1248});
end
clear fa18_pc

load ../zLibrary/mig29_pc;  %load mig29 section of library
for index=1457:1664  %for the mig29 section of the output_array
   output_array(index) = howCorrP(signal,mig29_pc{index-1456});
end
clear mig29_pc

load ../zLibrary/su27_pc;  %load su27 section of library
for index=1665:1872  %for the su27 section of the output_array
   output_array(index) = howCorrP(signal,su27_pc{index-1664});
end
clear su27_pc

load ../zLibrary/uh60_pc;  %load uh60 section of library
for index=1873:2080  %for the uh60 section of the output_array
   output_array(index) = howCorrP(signal,uh60_pc{index-1872});
end
clear uh60_pc
```

```
% **********   howCorrP.m    **********
% LT Zachary Cole, USN
% Naval Postgraduate School - Physics

% This file includes the definition of the howNear function.
% howNear determines how closely the test signal matches the library
% signal.

% input: test signal <256x1> and library signal <256x1>
% output: corr coef between 0 and 1

function result = howCorrP(testsig,librarysig);

result = max(xcorr(abs(testsig),abs(librarysig)))*256;


% **********   bi_corr_sim.m    **********
% LT Zachary Cole, USN
% Naval Postgraduate School - Physics

% RUN TIME: 40 Hours

% This file implements a cross correlation classification scheme
% for Bispectrum data.

% This is the general program control flow for running the bispectrum
% simulation.  It is broken up into 4 main loops.  Before each loop the
% actual checking of the library is done with another function.  Inside the
% loop, the arrays produced are filtered for results.  This control
% organization differs from p_corr_sim in that the time complexity is
% reduced by decreasing inefficient code.  Time becomes an issue for this
% code and expect this file to take 40 hours to run completely on lab
% computers.  This can be run in quarters without difficulty.  It
% creates 6 output files, one for each loop and 2 for consolidating the
% different bin matrices.

% inputs:
% R_stock   same configs as library at angles far from library (1-2 deg)
% R_stock2  same configs as library at angles closer to library (<=1 deg)
% R_dirty   armed aircraft at angles corresponding to library (0 deg)
% R_dirty2  armed aircraft at same angles as stock2
% lookup_table  a text array for displaying user friendly results
% ../zLibrary/  holds the library of aircraft

% class_array -- a cell array of arrays of 2080 correlation coefficients
% from comparing each test case to the library.
% index -- the maximum corr coef in the array

% helper files: checkLibraryCORRBi.m, rowS.m, rowD.m, column.m,
% fillRowWithCoefs.m, howCorrBi.m

clear;

load lookup_table;

% these are the matrices for individual identifications
bin_matrix_s = zeros(10,10);
bin_matrix_s2 = zeros(10,10);
bin_matrix_d = zeros(10,10);
bin_matrix_d2 = zeros(10,10);

% these are the matrices for averaged correlation coefficients
coef_matrix_s = zeros(10,10);
coef_matrix_s2 = zeros(10,10);
coef_matrix_d = zeros(10,10);
coef_matrix_d2 = zeros(10,10);
```

```
load R_stock;  %load set of test cases
class_array = checkLibraryCORRBi(R_stock,50);  %perform all checks
out = fopen('bi_corr_stock_results.txt','wt');  %open file for results
fprintf(out, 'bi_stock corr tests\n');
for testcase = 1:50
   % find most likely aircraft
   index=find(class_array{testcase}==max(class_array{testcase}));
   % fill matrix with coefficients
   coef_matrix_s(rowS(testcase),:) = coef_matrix_s(rowS(testcase),:) + fillRowWithCoefs(class_array{testcase});
   % fill binary matrix with likely identification
   bin_matrix_s(rowS(testcase),column(index))=bin_matrix_s(rowS(testcase),column(index))+1;
   fprintf(out, '%3g   %s\n',testcase, lookup_table(index,:));
end
clear R_stock;
coef_matrix_s = coef_matrix_s / 5; %average matrix (5 cases per aircraft)
fclose(out);

load R_stock2;  %load set of test cases
class_array = checkLibraryCORRBi(R_stock2,50);  %perform all checks
out = fopen('bi_corr_stock2_results.txt','wt');  %open file for results
fprintf(out, 'bi_stock2 corr tests\n');
%sort array for results
for testcase = 1:50
   % find most likely aircraft
   index=find(class_array{testcase}==max(class_array{testcase}));
   % fill matrix with coefficients
   coef_matrix_s2(rowS(testcase),:) = coef_matrix_s2(rowS(testcase),:) + fillRowWithCoefs(class_array{testcase});
   % fill binary matrix with likely identification
   bin_matrix_s2(rowS(testcase),column(index))=bin_matrix_s2(rowS(testcase),column(index))+1;
   fprintf(out, '%3g   %s\n',testcase, lookup_table(index,:));
end
clear R_stock2;
coef_matrix_s2 = coef_matrix_s2 / 5; %average matrix (5 cases per aircraft)
fclose(out);

load R_dirty;  %load set of test cases
class_array = checkLibraryCORRBi(R_dirty,45);  %perform all checks
out = fopen('bi_corr_dirty_results.txt','wt');  %open file for results
fprintf(out, 'bi_dirty corr tests\n');
for testcase = 1:45
   % find most likely aircraft
   index=find(class_array{testcase}==max(class_array{testcase}));
   % fill matrix with coefficients
   coef_matrix_d(rowD(testcase),:) = coef_matrix_d(rowD(testcase),:) + fillRowWithCoefs(class_array{testcase});
   % fill binary matrix with likely identification
   bin_matrix_d(rowD(testcase),column(index))=bin_matrix_d(rowD(testcase),column(index))+1;
   fprintf(out, '%3g   %s\n',testcase, lookup_table(index,:));
end
clear R_dirty;
coef_matrix_d = coef_matrix_d / 5; %average matrix (5 cases per aircraft)
fclose(out);

load R_dirty2;  %load set of test cases
class_array = checkLibraryCORRBi(R_dirty2,45);  %perform all checks
out = fopen('bi_corr_dirty2_results.txt','wt');  %open file for results
fprintf(out, 'bi_dirty2 corr tests\n');
for testcase = 1:45
   % find most likely aircraft
   index=find(class_array{testcase}==max(class_array{testcase}));
   % fill matrix with coefficients
   coef_matrix_d2(rowD(testcase),:) = coef_matrix_d2(rowD(testcase),:) + fillRowWithCoefs(class_array{testcase});
   % fill binary matrix with likely identification
   bin_matrix_d2(rowD(testcase),column(index))=bin_matrix_d2(rowD(testcase),column(index))+1;
   fprintf(out, '%3g   %s\n',testcase, lookup_table(index,:));
end
clear R_dirty2;
coef_matrix_d2 = coef_matrix_d2 / 5; %average matrix (5 cases per aircraft)
fclose(out);
```

```
% Consolidate and print results to a file
% results will be matrices where rows correspond to test case platforms (5
% each) and columns correspond to library identifications by aircraft type.
out = fopen('bi_matrix_bin.txt','wt');
fprintf(out, 'bi_stock corr tests\n\n');
fprintf(out, 'A320 EA6B F4   F14  F15  F16  FA18 MiG  Su27 UH60\n');
fprintf(out, '%1.0f   %1.0f   %1.0f   %1.0f   %1.0f   %1.0f   %1.0f   %1.0f   %1.0f   %1.0f  \n', bin_matrix_s');
fprintf(out, '\nbi_stock2 corr tests\n\n');
fprintf(out, 'A320 EA6B F4   F14  F15  F16  FA18 MiG  Su27 UH60\n');
fprintf(out, '%1.0f   %1.0f   %1.0f   %1.0f   %1.0f   %1.0f   %1.0f   %1.0f   %1.0f   %1.0f  \n', bin_matrix_s2');
fprintf(out, '\nbi_dirty corr tests\n\n');
fprintf(out, 'A320 EA6B F4   F14  F15  F16  FA18 MiG  Su27 UH60\n');
fprintf(out, '%1.0f   %1.0f   %1.0f   %1.0f   %1.0f   %1.0f   %1.0f   %1.0f   %1.0f   %1.0f  \n', bin_matrix_d');
fprintf(out, '\nbi_dirty2 corr tests\n\n');
fprintf(out, 'A320 EA6B F4   F14  F15  F16  FA18 MiG  Su27 UH60\n');
fprintf(out, '%1.0f   %1.0f   %1.0f   %1.0f   %1.0f   %1.0f   %1.0f   %1.0f   %1.0f   %1.0f  \n', bin_matrix_d2');
fclose(out);

% Consolidate and print results to a file
out = fopen('bi_matrix_coef.txt','wt');
fprintf(out, 'bi_stock corr tests\n\n');
fprintf(out, 'A320   EA6B   F4    F14    F15    F16    FA18   MiG    Su27   UH60\n');
fprintf(out, '%5.4f %5.4f %5.4f %5.4f %5.4f %5.4f %5.4f %5.4f %5.4f %5.4f\n', coef_matrix_s');
fprintf(out, '\nbi_stock2 corr tests\n\n');
fprintf(out, 'A320   EA6B   F4    F14    F15    F16    FA18   MiG    Su27   UH60\n');
fprintf(out, '%5.4f %5.4f %5.4f %5.4f %5.4f %5.4f %5.4f %5.4f %5.4f %5.4f\n', coef_matrix_s2');
fprintf(out, '\nbi_dirty corr tests\n\n');
fprintf(out, 'A320   EA6B   F4    F14    F15    F16    FA18   MiG    Su27   UH60\n');
fprintf(out, '%5.4f %5.4f %5.4f %5.4f %5.4f %5.4f %5.4f %5.4f %5.4f %5.4f\n', coef_matrix_d');
fprintf(out, '\nbi_dirty2 corr tests\n\n');
fprintf(out, 'A320   EA6B   F4    F14    F15    F16    FA18   MiG    Su27   UH60\n');
fprintf(out, '%5.4f %5.4f %5.4f %5.4f %5.4f %5.4f %5.4f %5.4f %5.4f %5.4f\n', coef_matrix_d2');
fclose(out);


% ********************   checkLibraryCORRBi.m    **********************
% LT Zachary Cole, USN
% Naval Postgraduate School - Physics

% RUN TIME: 10 Hours

% checkLibrary is a function that provides an array where each element
% indicates how similiar the signal is to the specific library signal.
% The array element corresponds to a lookup table of all the library
% signals.  It must be done one part of the library at a time since loading
% the entire library would require 8GB of RAM.

% R-tests is now a cell array of the 2D Fourier transforms of the test
% cases with num being the number of test cases contained in the the cell
% array.  Pre-transformed for speed.

% Function flow loads the bispectrum array of 208 profiles for each
% aircraft one by one and compares each of the library profiles with all
% test cases.  output_array becomes a cell array where each cell is an
% array of correlation coefficients for that test case against all library
% instances.  The fft2 is not fftshifted because the result is not effected
% by the change.

% each aircraft_bic is over 700MB

function output_array = checkLibraryCORRBi(R_tests,num);

load ../zLibrary/a320_bic;  %load a320 section of library
for index=1:208  %for the a320 section of the output_array
   Rlib = fft2(abs(a320_bic{index}));
   %compare this library case to all test cases
   for test=1:num
```

```
      output_array{test}(index) = howCorrBi(R_tests{test},Rlib);
   end
end
clear a320_bic;

load ../zLibrary/ea6b_bic;  %load ea6b section of library
for index=209:416  %for the ea6b section of the output_array
   Rlib = fft2(abs(ea6b_bic{index-208}));
   %compare this library case to all test cases
   for test=1:num
      output_array{test}(index) = howCorrBi(R_tests{test},Rlib);
   end
end
clear ea6b_bic;

load ../zLibrary/f4_bic;  %load f4 section of library
for index=417:624  %for the f4 section of the output_array
   Rlib = fft2(abs(f4_bic{index-416}));
   %compare this library case to all test cases
   for test=1:num
      output_array{test}(index) = howCorrBi(R_tests{test},Rlib);
   end
end
clear f4_bic;

load ../zLibrary/f14_bic;  %load f14 section of library
for index=625:832  %for the f14 section of the output_array
   Rlib = fft2(abs(f14_bic{index-624}));
   %compare this library case to all test cases
   for test=1:num
      output_array{test}(index) = howCorrBi(R_tests{test},Rlib);
   end
end
clear f14_bic;

load ../zLibrary/f15_bic;  %load f15 section of library
for index=833:1040  %for the f15 section of the output_array
   Rlib = fft2(abs(f15_bic{index-832}));
   %compare this library case to all test cases
   for test=1:num
      output_array{test}(index) = howCorrBi(R_tests{test},Rlib);
   end
end
clear f15_bic;

load ../zLibrary/f16_bic;  %load f16 section of library
for index=1041:1248  %for the f16 section of the output_array
   Rlib = fft2(abs(f16_bic{index-1040}));
   %compare this library case to all test cases
   for test=1:num
      output_array{test}(index) = howCorrBi(R_tests{test},Rlib);
   end
end
clear f16_bic;

load ../zLibrary/fa18_bic;  %load fa18 section of library
for index=1249:1456  %for the fa18 section of the output_array
   Rlib = fft2(abs(fa18_bic{index-1248}));
   %compare this library case to all test cases
   for test=1:num
      output_array{test}(index) = howCorrBi(R_tests{test},Rlib);
   end
end
clear fa18_bic;

load ../zLibrary/mig29_bic;  %load mig29 section of library
for index=1457:1664  %for the mig29 section of the output_array
   Rlib = fft2(abs(mig29_bic{index-1456}));
```

```
   %compare this library case to all test cases
   for test=1:num
      output_array{test}(index) = howCorrBi(R_tests{test},Rlib);
   end
end
clear mig29_bic;

load ../zLibrary/su27_bic;  %load su27 section of library
for index=1665:1872  %for the su27 section of the output_array
   Rlib = fft2(abs(su27_bic{index-1664}));
   %compare this library case to all test cases
   for test=1:num
      output_array{test}(index) = howCorrBi(R_tests{test},Rlib);
   end
end
clear su27_bic;

load ../zLibrary/uh60_bic;  %load uh60 section of library
for index=1873:2080  %for the uh60 section of the output_array
   Rlib = fft2(abs(uh60_bic{index-1872}));
   %compare this library case to all test cases
   for test=1:num
      output_array{test}(index) = howCorrBi(R_tests{test},Rlib);
   end
end
clear uh60_bic;


% **********   howCorrBi.m    **********
% LT Zachary Cole, USN
% Naval Postgraduate School - Physics

% howCorrBi determines how closely the test signal matches the library
% signal.  Inputs are 2D Fourier transforms of bispectra

% input: test bicorr <511x511> and library bicorr <511x511>
% output: corr coef between 0 and 1

function result = howCorrBi(Rtest,Rlib);

%implements equation (15) from chapter V

denominator = sqrt(sum(sum(Rtest.*conj(Rtest))))*sqrt(sum(sum(Rlib.*conj(Rlib))));

ccoef = ifft2(Rtest.*conj(Rlib))/denominator;

result = abs(max(max(ccoef)))*511*511;


% **********   fillRowWithCoefs.m    **********
% LT Zachary Cole, USN
% Naval Postgraduate School - Physics

% this puts the max correlation coefficient for each
% aircraft type into the appropriate place in the matrix row.

function result = fillRowWithCoefs(arr);

result = zeros(1,10);

if length(arr) == 2080  %if stock cases
   result(1) = max(arr(1:208)); %max of a320 checks
   result(2) = max(arr(209:416)); %max of ea6b checks
   result(3) = max(arr(417:624)); %max of f4 checks
   result(4) = max(arr(625:832)); %max of f14 checks
   result(5) = max(arr(833:1040)); %max of f15 checks
   result(6) = max(arr(1041:1248)); %max of f16 checks
   result(7) = max(arr(1249:1456)); %max of fa18 checks
```

```
   result(8) = max(arr(1457:1664)); %max of mig29 checks
   result(9) = max(arr(1665:1872)); %max of su27 checks
   result(10) = max(arr(1873:2080)); %max of uh60 checks
end

if length(arr) == 1872  %if dirty cases
   result(2) = max(arr(1:208)); %max of ea6b checks
   result(3) = max(arr(209:416)); %max of f4 checks
   result(4) = max(arr(417:624)); %max of f14 checks
   result(5) = max(arr(625:832)); %max of f15 checks
   result(6) = max(arr(833:1040)); %max of f16 checks
   result(7) = max(arr(1041:1248)); %max of fa18 checks
   result(8) = max(arr(1249:1456)); %max of mig29 checks
   result(9) = max(arr(1457:1664)); %max of su27 checks
   result(10) = max(arr(1665:1872)); %max of uh60 checks
end


% ********************   column.m    **********************
% LT Zachary Cole, USN
% Naval Postgraduate School - Physics

% simple function to convert the index to a column for the confusion matrix
% the index corresponds to a specific aircraft's area of the array.
% result is the number of the library aircraft.

function result = column(index);

if index <= 208
   result = 1; %a320
elseif index <= 416
   result = 2; %ea6b
elseif index <= 624
   result = 3; %f4
elseif index <= 832
   result = 4; %f14
elseif index <= 1040
   result = 5; %f15
elseif index <= 1248
   result = 6; %f16
elseif index <= 1456
   result = 7; %fa18
elseif index <= 1664
   result = 8; %mig29
elseif index <= 1872
   result = 9; %su27
else
   result = 10; %uh60
end


% ********************   rowS.m    **********************
% LT Zachary Cole, USN
% Naval Postgraduate School - Physics

% converts the testcase variable to a row on the column matrix for the
% stock test cases

function result = rowS(test);

if test <= 5
   result = 1; %a320
elseif test <= 10
   result = 2; %ea6b
elseif test <= 15
   result = 3; %f4
elseif test <= 20
   result = 4; %f14
```

```
elseif test <= 25
   result = 5; %f15
elseif test <= 30
   result = 6; %f16
elseif test <= 35
   result = 7; %fa18
elseif test <= 40
   result = 8; %mig29
elseif test <= 45
   result = 9; %su27
else
   result = 10; %uh60
end


% ********************  rowD.m  **********************
% LT Zachary Cole, USN
% Naval Postgraduate School - Physics

% converts the testcase variable to a row on the column matrix for the
% dirty test cases

function result = rowD(test);

if test <= 5
   result = 2; %ea6b
elseif test <= 10
   result = 3; %f4
elseif test <= 15
   result = 4; %f14
elseif test <= 20
   result = 5; %f15
elseif test <= 25
   result = 6; %f16
elseif test <= 30
   result = 7; %fa18
elseif test <= 35
   result = 8; %mig29
elseif test <= 40
   result = 9; %su27
else
   result = 10; %uh60
end
```

E. INDIVIDUAL SIMULATION RESULTS

High Bandwidth Results:

```
p_stock corr tests

     A320 EA6B F4   F14  F15  F16  FA18 MiG  Su27 UH60
A320 4    0    1    0    0    0    0    0    0    0
EA6B 1    4    0    0    0    0    0    0    0    0
  F4 0    0    3    0    1    0    0    0    0    1
 F14 0    0    0    3    0    0    1    0    0    1
 F15 1    0    0    1    2    0    1    0    0    0
 F16 0    0    0    0    0    4    0    0    1    0
FA18 1    0    0    1    1    1    1    0    0    0
 MiG 0    0    0    0    0    1    1    3    0    0
Su27 1    0    1    0    0    1    0    0    2    0
UH60 0    0    1    0    0    0    0    0    0    4

p_stock2 corr tests
```

```
     A320 EA6B F4   F14  F15  F16  FA18 MiG  Su27 UH60
A320 3    1    1    0    0    0    0    0    0    0
EA6B 0    5    0    0    0    0    0    0    0    0
  F4 0    0    4    0    0    0    1    0    0    0
 F14 0    0    0    3    0    0    1    0    0    1
 F15 0    0    0    0    3    0    0    1    0    1
 F16 0    0    0    0    0    2    1    0    1    1
FA18 0    0    1    0    0    1    2    0    0    1
 MiG 0    0    1    1    0    1    0    2    0    0
Su27 0    0    0    0    0    0    0    1    4    0
UH60 0    0    1    0    0    1    1    0    0    2
```

p_dirty corr tests

```
     A320 EA6B F4   F14  F15  F16  FA18 MiG  Su27 UH60
A320 0    0    0    0    0    0    0    0    0    0
EA6B 0    5    0    0    0    0    0    0    0    0
  F4 0    0    2    0    2    0    1    0    0    0
 F14 0    0    0    3    1    1    0    0    0    0
 F15 0    0    1    1    3    0    0    0    0    0
 F16 0    0    0    0    0    4    1    0    0    0
FA18 0    0    0    0    0    1    3    0    0    1
 MiG 0    0    0    0    0    0    0    5    0    0
Su27 0    0    0    0    0    0    0    0    5    0
UH60 0    0    2    0    0    0    0    0    0    3
```

p_dirty2 corr tests

```
     A320 EA6B F4   F14  F15  F16  FA18 MiG  Su27 UH60
A320 0    0    0    0    0    0    0    0    0    0
EA6B 0    4    0    0    0    0    0    1    0    0
  F4 0    0    0    0    0    2    1    2    0    0
 F14 0    0    2    1    0    0    0    1    0    1
 F15 0    0    0    1    0    1    1    1    1    0
 F16 0    0    0    2    0    1    1    1    0    0
FA18 0    1    1    0    0    1    1    0    0    1
 MiG 0    0    3    0    0    1    0    1    0    0
Su27 0    0    0    0    0    1    0    0    4    0
UH60 0    0    1    0    1    0    3    0    0    0
```

bi_stock corr tests

```
     A320 EA6B F4   F14  F15  F16  FA18 MiG  Su27 UH60
A320 2    3    0    0    0    0    0    0    0    0
EA6B 0    3    0    0    0    1    0    0    0    1
  F4 0    0    2    1    0    0    1    0    0    1
 F14 0    0    1    4    0    0    0    0    0    0
 F15 0    0    0    0    3    0    1    0    0    1
 F16 0    0    0    1    0    3    0    0    0    1
FA18 0    0    0    0    0    0    4    1    0    0
 MiG 0    0    0    1    0    0    0    3    0    1
Su27 0    0    0    1    1    1    0    0    1    1
UH60 0    0    1    0    0    0    0    0    0    4
```

bi_stock2 corr tests

```
     A320 EA6B F4   F14  F15  F16  FA18 MiG  Su27 UH60
A320 3    1    1    0    0    0    0    0    0    0
EA6B 0    5    0    0    0    0    0    0    0    0
  F4 1    0    4    0    0    0    0    0    0    0
 F14 0    0    0    4    0    1    0    0    0    0
```

```
 F15 0    0    0    1    4    0    0    0    0    0
 F16 0    0    0    0    0    4    0    0    0    1
FA18 0    1    0    0    0    1    3    0    0    0
 MiG 0    0    0    1    0    0    0    4    0    0
Su27 0    0    0    1    0    0    0    0    4    0
UH60 0    0    0    0    0    0    0    0    0    5
```

```
bi_dirty corr tests
```

```
     A320 EA6B F4   F14  F15  F16  FA18 MiG  Su27 UH60
A320 0    0    0    0    0    0    0    0    0    0
EA6B 0    5    0    0    0    0    0    0    0    0
  F4 0    0    5    0    0    0    0    0    0    0
 F14 0    0    0    4    0    1    0    0    0    0
 F15 0    0    0    0    5    0    0    0    0    0
 F16 0    0    0    0    0    4    1    0    0    0
FA18 0    0    1    1    0    1    1    0    0    1
 MiG 0    0    0    0    0    0    0    5    0    0
Su27 0    0    0    0    0    0    0    0    5    0
UH60 0    0    0    0    0    3    0    0    0    2
```

```
bi_dirty2 corr tests
```

```
     A320 EA6B F4   F14  F15  F16  FA18 MiG  Su27 UH60
A320 0    0    0    0    0    0    0    0    0    0
EA6B 0    5    0    0    0    0    0    0    0    0
  F4 0    0    1    0    0    1    0    1    0    2
 F14 0    1    0    3    0    1    0    0    0    0
 F15 0    2    0    2    0    1    0    0    0    0
 F16 0    0    0    0    0    4    1    0    0    0
FA18 0    0    2    0    0    0    2    1    0    0
 MiG 0    0    1    0    0    0    1    3    0    0
Su27 1    0    0    0    0    0    1    0    3    0
UH60 0    0    1    0    1    0    2    0    0    1
```

Low Bandwidth Results:

```
p_stock corr tests
```

```
     A320 EA6B F4   F14  F15  F16  FA18 MiG  Su27 UH60
A320 3    0    0    0    1    0    0    0    1    0
EA6B 0    4    0    0    1    0    0    0    0    0
  F4 0    0    3    1    0    0    0    1    0    0
 F14 0    0    0    3    0    1    1    0    0    0
 F15 0    0    1    0    1    0    0    3    0    0
 F16 0    0    0    0    1    1    1    1    0    1
FA18 0    0    0    0    1    0    1    1    0    2
 MiG 0    0    2    0    1    1    0    1    0    0
Su27 0    0    0    1    1    0    1    0    1    1
UH60 0    0    1    0    1    1    0    0    0    2
```

```
p_stock2 corr tests
```

```
     A320 EA6B F4   F14  F15  F16  FA18 MiG  Su27 UH60
A320 4    0    0    0    0    0    0    0    0    1
EA6B 0    4    0    0    1    0    0    0    0    0
  F4 0    0    3    0    0    0    0    2    0    0
 F14 0    0    0    2    0    2    1    0    0    0
 F15 0    0    0    0    3    1    0    1    0    0
 F16 0    0    0    0    1    1    0    1    1    1
FA18 0    0    1    0    0    0    1    2    0    1
```

```
 MiG 0    0    2    0    1    0    1    0    0    1
Su27 0    0    1    0    1    0    0    0    2    1
UH60 0    0    0    0    1    0    0    0    0    4
```

p_dirty corr tests

```
     A320 EA6B F4   F14  F15  F16  FA18 MiG  Su27 UH60
A320 0    0    0    0    0    0    0    0    0    0
EA6B 0    5    0    0    0    0    0    0    0    0
  F4 1    0    2    1    0    1    0    0    0    0
 F14 0    0    1    4    0    0    0    0    0    0
 F15 0    0    1    1    2    0    0    0    0    1
 F16 0    0    0    0    0    3    1    1    0    0
FA18 1    0    0    0    0    0    2    1    1    0
 MiG 0    0    0    0    0    0    0    5    0    0
Su27 0    0    0    0    0    0    0    0    5    0
UH60 0    1    0    0    0    0    0    0    0    4
```

p_dirty2 corr tests

```
     A320 EA6B F4   F14  F15  F16  FA18 MiG  Su27 UH60
A320 0    0    0    0    0    0    0    0    0    0
EA6B 0    4    0    0    1    0    0    0    0    0
  F4 0    0    2    0    1    1    0    0    0    1
 F14 0    0    0    3    0    2    0    0    0    0
 F15 0    0    0    0    3    0    0    1    1    0
 F16 0    0    1    1    0    0    1    0    1    1
FA18 0    0    0    0    2    0    0    1    2    0
 MiG 1    0    1    0    0    1    2    0    0    0
Su27 0    0    1    1    2    0    0    0    1    0
UH60 1    0    1    0    0    0    0    0    0    3
```

bi_stock corr tests

```
     A320 EA6B F4   F14  F15  F16  FA18 MiG  Su27 UH60
A320 3    0    0    0    0    0    0    0    0    2
EA6B 0    5    0    0    0    0    0    0    0    0
  F4 0    0    3    0    1    1    0    0    0    0
 F14 0    0    0    3    0    1    1    0    0    0
 F15 0    0    0    1    0    1    0    2    1    0
 F16 0    0    0    1    1    3    0    0    0    0
FA18 0    0    0    0    1    1    3    0    0    0
 MiG 0    0    1    0    0    0    1    3    0    0
Su27 0    0    0    1    0    0    0    0    4    0
UH60 0    0    1    0    0    0    2    1    0    1
```

bi_stock2 corr tests

```
     A320 EA6B F4   F14  F15  F16  FA18 MiG  Su27 UH60
A320 3    1    0    0    0    0    1    0    0    0
EA6B 0    4    0    0    0    0    1    0    0    0
  F4 0    0    2    2    0    1    0    0    0    0
 F14 0    0    0    2    1    2    0    0    0    0
 F15 0    0    0    0    2    3    0    0    0    0
 F16 0    0    0    0    1    2    1    1    0    0
FA18 0    0    1    0    0    1    1    1    0    1
 MiG 1    0    0    0    1    2    0    0    0    1
Su27 0    0    0    0    0    1    0    0    4    0
UH60 0    1    1    0    1    1    0    0    0    1
```

bi_dirty corr tests

	A320	EA6B	F4	F14	F15	F16	FA18	MiG	Su27	UH60
A320	0	0	0	0	0	0	0	0	0	0
EA6B	0	5	0	0	0	0	0	0	0	0
F4	0	0	2	0	0	2	0	0	1	0
F14	0	0	1	4	0	0	0	0	0	0
F15	0	0	0	0	5	0	0	0	0	0
F16	0	0	0	0	0	5	0	0	0	0
FA18	0	0	1	0	2	0	1	1	0	0
MiG	0	0	0	0	0	0	0	5	0	0
Su27	0	0	0	0	0	0	0	0	5	0
UH60	0	0	1	0	0	2	1	0	0	1

bi_dirty2 corr tests

	A320	EA6B	F4	F14	F15	F16	FA18	MiG	Su27	UH60
A320	0	0	0	0	0	0	0	0	0	0
EA6B	0	4	0	0	1	0	0	0	0	0
F4	0	0	1	0	1	2	0	1	0	0
F14	0	1	0	2	0	1	1	0	0	0
F15	0	0	2	0	1	0	0	0	2	0
F16	0	0	0	1	1	2	1	0	0	0
FA18	0	0	2	0	0	1	1	0	1	0
MiG	1	0	1	0	1	0	0	1	1	0
Su27	0	0	0	1	0	0	0	0	4	0
UH60	0	0	1	1	0	0	1	0	0	2

THIS PAGE INTENTIONALLY LEFT BLANK

LIST OF REFERENCES

[1] D. Evans, "Vincennes: a case study," *Proceedings*, pp. 49-55, August 1993.

[2] GlobalSecurity.org, "Operation Provide Comfort II," April 2007, http://www.globalsecurity.org/military/ops/provide_comfort_2.htm.

[3] CBS News, "The Patriot Flawed?" April 2007, http://www.cbsnews.com/stories/2004/02/19/60minutes/main601241.shtml.

[4] B. T. Neale, "CH – the first operational radar," *GEC Journal of Research*, vol. 3, no. 2, pp. 73-83, 1985.

[5] B. Borden, *Radar Imaging of Airborne Targets*. Philadelphia: Institute of Physics Publishing, 1999.

[6] "Physics of active electromagnetic detection and engagement," class notes for PH4274, Department of Physics, Naval Postgraduate School, Summer 2006.

[7] "Physics of advanced imaging systems," class notes for PH4273, Department of Physics, Naval Postgraduate School, Fall 2006.

[8] J. M. Anderson, "Nonlinear suppression of range ambiguity in pulse Doppler radar," Ph.D. dissertation, Air Force Institute of Technology, Ohio, 2001.

[9] R. J. Sullivan, *Microwave Radar*. Boston: Artech House, 2000.

[10] D. J. Griffiths, *Introduction to Electrodynamics*. New Jersey: Prentice Hall, 1999.

[11] J. W. Yeo, "Bi-spectral method for radar target recognition," M.S. thesis, Naval Postgraduate School, Monterey, CA, 2006.

[12] W. Panofsky and M. Phillips, *Classical Electricity and Magnetism*. New York: Dover Publications, 1990.

[13] "Topics in advanced electricity and magnetism," class notes for PH4353, Department of Physics, Naval Postgraduate School, Winter 2007.

[14] B. Borden, "Radar," unpublished notes, Department of Physics, Naval Postgraduate School, September 2006.

[15] J. S. Asvestas, "The physical optics method in electromagnetic scattering," *Journal of Mathematical Physics*, vol. 21, pp. 290-299, February 1980.

[16] P. Y. Ufimtsev, *Fundamentals of the Physical Theory of Diffraction*. New Jersey: John Wiley & Sons, March 2007.

[17] R. Bhalla and H. Ling, "A fast algorithm for signature prediction and image formation using the shooting and bouncing ray technique," in *Antennas and Propagation Society International Symposium*, 1994, pp. 1990-1993.

[18] Tripoint Industries Technical Staff, *User's Manual for Lucernhammer*, Tripoint Industries, 2005.

[19] A. Ferhat, Bilkent University, "UTD applet," April 2007, http://www.cem.bilkent.edu.tr/UTD/Utd.htm.

[20] 551 and 552 AEW&C Wings, U.S. Air Force, "Identification friend or foe (IFF) systems," April 2007, http://www.dean-boys.com/extras/iff/iffqa.html.

[21] K. Nelson (Kyle_Nelson30@hotmail.com), "AN/SPS-49 naval air surveillance radar," April 2007, http://www.turbosquid.com/Preview.

[22] P. Tait, *Introduction to Radar Target Recognition*, United Kingdom: Institution of Engineering and Technology, 2006.

[23] R. Van Der Heigen, "Aircraft recognition with radar range profiles," Ph.D. dissertation, University of Amsterdam, Netherlands, 1998.

[24] I. Jouny, R. L. Moses, and F. D. Garber, "Classification of radar signals using the bispectrum," in *International Conference on Acoustics, Speech, and Signal Processing*, 1991, pp. 14-17.

[25] I. Jouny, "Description of radar targets using the bispectrum," *IEE Proceedings – Radar, Sonar and Navigation*, vol. 141, pp. 159-163, June 1994.

[26] I. Jouny, F. D. Garber, and R. L. Moses, "Radar target identification using the bispectrum: a comparative study," *IEEE Transactions on Aerospace and Electronic Systems*, vol. 31, pp. 66-77, January 1995.

[27] J. Spoelstra and E. C. Botha, "Radar target recognition using multiple bounce scattering terms," in *Proceedings of the 1992 South African Symposium on Communications and Signal Processing*, 1992, pp. 17-21.

[28] E. K. Walton and I. Jouny, "Bispectrum of radar signatures and application to target classification," *Radio Science*, vol 25, pp. 101-113, August 1990.

[29] 3D Model CD-ROM Set, Mesh Factory, Defiance, OH.

INITIAL DISTRIBUTION LIST

1. Defense Technical Information Center
   Ft. Belvoir, Virginia

2. Dudley Knox Library
   Naval Postgraduate School
   Monterey, California

3. Professor Brett Borden
   Physics Department
   Naval Postgraduate School
   Monterey, California

4. Professor Donald L. Walters
   Physics Department
   Naval Postgraduate School
   Monterey, California

5. Chairman, Physics Department
   Naval Postgraduate School
   Monterey, California

6. LT Zachary K. Cole
   United States Navy
   Chantilly, Virginia